This thesis in electronic version is provided to the Library by the author. In the case where its contents is different from the printed version, the printed version shall prevail.

# TRANSDERMAL MICRONEEDLES PATCH FOR PAINLESS AND REGULATED DRUG DELIVERY ACROSS SKIN

# WONG WAI KIT ANTHONY

# M.PHIL

THE HONG KONG
POLYTECHNIC UNIVERSITY
2014

# The Hong Kong Polytechnic University Interdisciplinary Division of Biomedical Engineering

Transdermal Microneedles Patch for Painless and
Regulated Drug Delivery across Skin
by

WONG Wai Kit Anthony

A thesis submitted in partial fulfillment of the requirements for the degree of Master of Philosophy

August 2013

# **Certificate of Originality**

I hereby declare that this thesis is my own work and	that, to the best of my knowledge
and belief, it reproduces no material previously pub	lished or written, nor material tha
has been accepted for the award of any other degree	ree or diploma, except where due
acknowledgement has been made in the text.	
	(Signed)
	(Signed)
Mr. WONG Wai Kit Anthony	(Name of Author)

# Acknowledgements

This project cannot be completed without the supervision of and inspiration by Dr. Thomas Lee. I am heartily thankful to his patient guidance, invaluable advices, and heartfelt encouragement throughout my study. I would also like to express my great gratitude to my colleagues in laboratory S106B for their support and beneficial discussion. My deepest gratitude is also given to Prof. K. L. Yeung and Mr. Timothy Poon at The Hong Kong University of Science and Technology, Prof. K. L. Yung and Dr. Matthew Kwan at The Hong Kong Polytechnic University for providing zeolite and plastic microneedle arrays, respectively. The generous help from Mr. Blizzard Chau at The Chinese University of Hong Kong in animal study is highly appreciated. I also wholeheartedly thank the staffs in Design and Manufacturing Service Facility at The Hong Kong University of Science and Technology for the rapid prototyping. Besides, I would like to take this opportunity to thank all others who give their hands and support to me in various aspects. Last but not least, I wish to avail myself of this opportunity to express a sense of sincere gratitude and love to my friends, my beloved family, and fianc & for their unconditional love, support, and understanding throughout my life.

# **Abstract**

Transdermal patch has become a promising way of drug delivery with low potential risks in past decades. Its simplicity, high portability, low cost, and minimal medical hazardous generation has led to high patient compliance and prevention of disease transmission. Typically, the reservoir and matrix systems allow drug diffusion through the skin barrier to microcirculation in the dermis. Undesirably, the unique closely packed cell structure of the stratum corneum inhibits the passage of a wide variety of drugs that are commonly used in current therapies. The concentration dependence of drug diffusion in conventional patch design also makes sustained delivery difficult. In view of this, recent research has put emphasis on bypassing the stratum corneum so as to allow more drugs to be delivered via the transdermal route. One major challenge is to achieve continuous drug delivery while keeping the device portable and simple. Herein, a microneedle-bonded transdermal patch with dimensions of less than 4 mm in height and 25 mm in diameter is developed, with the drug delivery rate controlled by a hydrogel actuator. The swelling rate of the hydrogel depends on the presence of swelling agent and number of PDMS coating on the hydrogel. Results show that the device can

successfully deliver diverse drugs steadily in 8 hours using in vitro diffusion cell model. Furthermore, with insulin delivery to diabetic rats, the transdermal patch renders comparable glucose lowering effect as the intradermal injection.

# **Table of Contents**

Certificate of Originality
Acknowledgementsii
Abstractiii
Table of Contentsv
List of Publicationsix
List of Figuresx
List of Tablesxv
List of Equationsxvi
List of Abbreviationsxvii
Introduction 1
1.1. Transdermal drug delivery
1.2. Physiology of the skin
1.3. General design of transdermal patch
1.4. Challenges in current transdermal patch design
1.5. Approaches in overcoming the barrier

1.5	5.1. Drug delivery by passive means	8
	1.5.1.1. Microneedles	11
1.5	5.2. Drug delivery by active means	14
	1.5.2.1. Iontophoresis	14
1.5	5.3. Combined use of the technologies	15
1.6. Co	ontinuous drug delivery	17
1.6	6.1. Delivery of insulin: a case study	18
1.6	6.2. Active infusion	23
1.7. Hy	ydrogel	26
1.7	7.1. Theoretical swelling studies	27
1.7	7.2. General applications	29
1.7	7.3. Applications as actuators	30
1.8. Ob	ojectives of the study	32
Research M	Methodology	34
2.1. Dru	rug delivery scheme	34
2.2. Ma	aterials and methods	36

	2.2.1. Materials and instrumentations	36
·	2.2.2. Synthesis of polyacrylamide-co-polyethylene glycol	38
	2.2.3. Spray coating of polydimethylsiloxane on hydrogel	39
	2.2.4. Synthesis of elastic polydimethylsiloxane membrane	41
	2.2.5. Design of the transdermal delivery patch	41
	2.2.6. Assembly of the transdermal patch	47
	2.2.7. Hydrogel swelling characterization	48
	2.2.8. Preparation of porcine ear back skin	49
	2.2.9. Skin insertion test	50
	2.2.10. Drug permeation test in vitro	50
	2.2.11. In vivo test	52
Results an	nd Discussion	54
3.1. V	Visualization of hydrogel swelling	54
3.2. S	Skin insertion tests by microneedles	58
3.3. I	In vitro drug permeation tests	63
:	3.3.1. In vitro test – methylene blue	63

3.3.2. In	vitro test – diclofenac sodium	67
3.3.3. In	vitro test – FITC-insulin	70
3.3.4. Et	ffect of coating hydrogel with PDMS on drug delivery effic	ciency 72
3.3.5. Do	elivery of different drugs by P-O-500-bonded patch	75
3.4. In vivo to	est – insulin	77
3.5. Feasibilit	ty of scaling up production	78
Conclusions and	Recommendations for Future Work	81
4.1. Key find	ings and conclusions	81
4.2. Recomm	nendations for future work	82
References		84

# **List of Publications**

# **Patent Application**

• United States Provisional Patent US61/744636 "Design and manufacture of nonelectronic, active infusion patch and device for transdermal delivery across skin"

# Conferences

- 244<sup>th</sup> ACS National Meeting 2012 (Philadelphia)
- NanoTech 2011 & 2012 (Tokyo)

# **List of Figures**

Figure 1.1. A schematic view of the human skin (adopted from Advanced Drug Delivery
Reviews, vol. 65, pp. 152-168, 2013 [8])
Figure 1.2. Generalized designs of conventional transdermal patch (adopted from
European Journal of Pharmaceutics and Biopharmaceutics, vol. 64. pp. 1-8, 2006 [9]).6
Figure 1.3. Normal insulin responses to three high carbohydrate (3CHO), six high
carbohydrates (6CHO), and six high protein (6PRO) meals daily (adopted from the
European e-Journal of Clinical Nutrition and Metabloism, vol. 5, pp. 277-280, 2010 [54])
Figure 1.4. Pharmacokinetics of different insulin analogues in human (adopted from
American Journal of Management Care, vol. 13 Supplement 2, pp. 47-54, 2007 [55]).21
Figure 1.5. Expanded view of the heat-controlled drug delivery device (adopted from
IEEE Transactions on Biomedical Engineering, vol. 55, pp. 1063-1071, 2008 [58]) 24
Figure 1.6. A drug delivery device with an autonomous pump (adopted from
Macromolecular Symposia, vol. 210, pp. 377-384, 2004 [59])
<b>Figure 1.7.</b> A microdispensing device driven by a pressure pump (adopted from <i>Journal</i>

of Microelectromechanical Systems, vol. 13, pp. 586-593, 2004 [71])
<b>Figure 2.1.</b> Delivery scheme of drug in the microneedle-adhered transdermal patch 35
<b>Figure 2.2.</b> Spacer for hydrogel cutting
<b>Figure 2.3.</b> Polydimethylsiloxane (PDMS) spray coating setup
Figure 2.4. First generation - structures of (left) the insulin reservoir and (right) the water
and hydrogel reservoirs showing their dimensions and alignment feature. (Top)
Cross-sectional views across the dotted lines shown below and (bottom) surface views of
the structures
<b>Figure 2.5.</b> Expanded view of the first generation transdermal drug delivery patch 42
Figure 2.6. A prototype of the first generation assembled patch with stainless steel
microneedle (SSM-O-150)
Figure 2.7. Second generation - structures of (1) key; (2) backing cover; (3) turnable
cover; (4) swelling agent and hydrogel reservoirs; (5) insulin reservoir and (6) watch liked
patch holder showing their dimensions and alignment feature. (a) Cross-sectional views
across the dotted lines shown below and (b) surface views of the structures 44
<b>Figure 2.8.</b> Expanded view of the second generation transdermal drug delivery patch. 46

<b>Figure 2.9.</b> A prototype of the second generation assembled patch
<b>Figure 2.10.</b> Transparent substrate for hydrogel swelling characterization
<b>Figure 2.11.</b> Setup for hydrogel swelling characterization
Figure 2.12. Insulin-loaded second generation transdermal patch attached to a diabetes
milletus (DM)-induced rat
<b>Figure 3.1.</b> Swelling property of uncoated hydrogel swelling over time
Figure 3.2. Cross-sectional view of a polydiemthylsiloxane (PDMS)-coated hydrogel
under scanning electron micronscope (SEM)
<b>Figure 3.3.</b> Swelling properties of uncoated and coated hydrogel over time 57
Figure 3.4. [Left] stainless steel microneedle (ME-C-600) and [middle] plastic
microneedle (P-O-500) under camera, as well as [right] zeolite microneedle (SSM-O-150)
under scanning electron microscope (SEM)
Figure 3.5. Insertion test of the negative control when put [left] under (side of stratum
corneum facing) as well as [right] above (side of dermis facing) a lighting system 59
<b>Figure 3.6.</b> Insertion test of stainless steel microneedle (ME-C-600) when put [left] under
(side of stratum corneum facing) as well as [right] above (side of dermis facing) a

lighting system
<b>Figure 3.7.</b> Insertion test of zeolite microneedle (SSM-O-150) when put [left] under (side
of stratum corneum facing) as well as [right] above (side of dermis facing) a lighting
system61
Figure 3.8. Insertion test of plastic microneedle (P-O-500) when put [left] under (side of
stratum corneum facing) as well as [right] above (side of dermis facing) a lighting
system
<b>Figure 3.9.</b> Standard curve of methylene blue (MB)
Figure 3.10. In vitro tests using different types of microneedles: stainless steel
microneedle (ME-C-600), zeolite microneedle (SSM-O-150), or plastic mcironeedle
(P-O-500); and delivery mechanisms: diffusion (DF) or active infusion (AI)
<b>Figure 3.11.</b> A chromatogram of 100 $\mu$ g/ mL diclofenac sodium (DFS) sample 68
<b>Figure 3.12.</b> Standard curve of diclofenac sodium (DFS)
Figure 3.13. Cumulative release of diclofenac sodium (DFS) by patches with different
types of microneedles
<b>Figure 3.14.</b> Standard curve of fluoroscein-tagged insulin (FITC-insulin)

<b>Figure 3.15.</b> Cumulative release of fluoroscein-tagged insulin (FITC-insulin) by patches
with different types of microneedles. 72
Figure 3.16. Cumulative release of diclofenac sodium (DFS) by plastic microneedle
(P-O-500)-adhered patch loaded with hydrogel having different layers of
polydimethyljsiloxane (PDMS) coating
Figure 3.17. Cumulative release of different drugs by plastic microneedle
(P-O-500)-adhered patch76
Figure 3.18. Blood glucose level change in response to insulin administration by various
approaches
Figure 3.19. A cost estimation of patch made by injection molding (adopted from
http://www.custompartnet.com/estimate/injection-molding/ [86])

# **List of Tables**

Table 1. Fickian diffusion models and their time dependen	nce29
<b>Table 2.</b> Properties of different types of microneedles	58

# **List of Equations**

Equation 1.1. Steady state flux at equilibrium (adopted from European Journal of
Pharmaceutical Sciences, vol. 14, pp. 101-114, 2001 [10])
Equation 1.2. Daily insulin dose of a DM patient (adopted from
http://dtc.ucsf.edu/types-of-diabetes/type2/treatment-of-type-2-diabetes/medications-and
-therapies/type-2-insulin-rx/calculating-insulin-dose/#formulas [53])
<b>Equation 1.3.</b> Power law equation (adopted from <i>Journal of Controlled Release</i> , vol. 5
pp. 23-26, 1987 [66])

# **List of Abbreviations**

ACN acetonitrile

AI active infusion

BGL blood glucose level

DF diffusion

DFS diclofenac sodium

DM diabetes mellitus

EB evans blue

FITC-insulin fluorescein isothiocyanate-conjugated insulin

HIV human immunodeficiency virus

ID intradermal

MB methylene blue

PAAm polyacrylamide

PDMS polydimethylsiloxane

UPLC ultra performance liquid chromatography

# **Chapter 1**

# Introduction

Drugs have been used in medicinal purpose for thousands of years. One of the existing oldest medicinal recommendation of Chinese herbs was found in 2735 B.C. [1]. Conventional human drug delivery routes involve oral administration and parenteral (intravenous, intramuscular, and subcutaneous) injection in the past two centuries. The injection would, unfortunately, either generate medical hazardous waste that needs alternative disposal or encounter first pass effect that reduces bioavailability [2, 3]. Transdermal delivery, in contrast, has received considerable attention in the past two decades due to its ease of use, low cost, and high level of comfort [4]. Increasing transdermal products have been released to market in recent years thanks to the advance of pharmaceutical industry and chemical technology. In what follows, detailed background of transdermal drug delivery and skin physiology will be discussed in Section 1.1 and Section 1.2, respectively. The conventional transdermal patch design will be delineated in Section 1.3, followed by its drawback and limitations in Section 1.4. Recent approaches in overcoming the rate limiting barrier will be mentioned in Section 1.5. The importance of continuous drug delivery will be reviewed in Section 1.6. Hydrogel and its application will be introduced in Section 1.7. Finally, the objectives of the current study will be stated in Section 1.8.

# 1.1. Transdermal drug delivery

Transdermal delivery offers painless pathway without generation of any dangerous medical waste that poses a risk of blood borne disease transmission such as hepatitis B and human immunodeficiency virus (HIV) from needle reuse which is common in developing countries [5]. It eliminates risks of enzymatic degradation and poor drug adsorption in the gastrointestinal tract or liver that inhibit pharmacokinetics of drugs to be delivered. Transdermal delivery is also noninvasive or minimally invasive with capability of self-administration and high degree of patient compliance. It provides a low-cost drug delivery system with capacity for long-term controlled release. The United States Food and Drug Administration approved the first transdermal patch in 1981 for scopolamine, a drug that suppresses nausea and vomiting from motion sickness

[6]. In the United States market, more than 35 transdermal products were introduced during the past two decades, generating total sales of USD 5.7 billion in 2006. Some analysts predict the sales in the global market will be up to USD 32 billion in 2015. The rapid increase in the market value leads transdermal drug delivery to be one of the fastest growing sectors within the pharmaceutical industry.

# 1.2. Physiology of the skin

A general skin structure is composed of four layers, from top to bottom, as shown in Figure 1.1: stratum corneum of 10– $20~\mu m$  thickness; viable epidermis of approximately 700  $\mu m$ ; dermis of 1,500–3,000  $\mu m$ ; and subcutaneous fat. The stratum corneum is the outermost layer of the skin with high hydrophobicity. It was thought to be chemically and biologically noble until complex physiological interactions were discovered in the stratum corneum in the past few decades. Corneocytes, protein complexes enriched in water holding keratin, are adhered together by long-chain  $\alpha$ -hydroxyceramides. Packing of 10–15 layers of these dead cells assigns the barrier function of the skin that allows protection of the more active skin layer underneath [7].

Because of the well-organized structure, the stratum corneum is believed to be the major barrier to external stimuli and materials that intends to permeate across.

The viable epidermis is made of multiple layers of proliferating keratinocytes. Keratinocytes start to lose nuclei and change their compositions after mitosis, of which they are successively squeezed up to the stratum corneum until shredded eventually. Drug that passes across the stratum corneum is subjected to improved permeation through the epidermis from layer to layer, due to loosen orientation of cells with wide cellular junction. Other catabolic enzymes-containing cells, such as Langerhans cells, are also available in the epidermis. The presence of these cells gives a promising way to the therapeutic benefits of transdermal drug delivery.

The dermis serves as a cushion and provides elasticity to the skin due to the presence of collagen fibrils in the extracellular matrix. It also offers nourishment to cells in the dermis and epidermis by its embedded blood and lymph vessels. Anchored mechanoreceptors enable heat and touch sensing to adapt environmental changes. Moreover, the dermis contains hair follicles which are targeted as a route of drug penetration, so-called the transappendageal route.

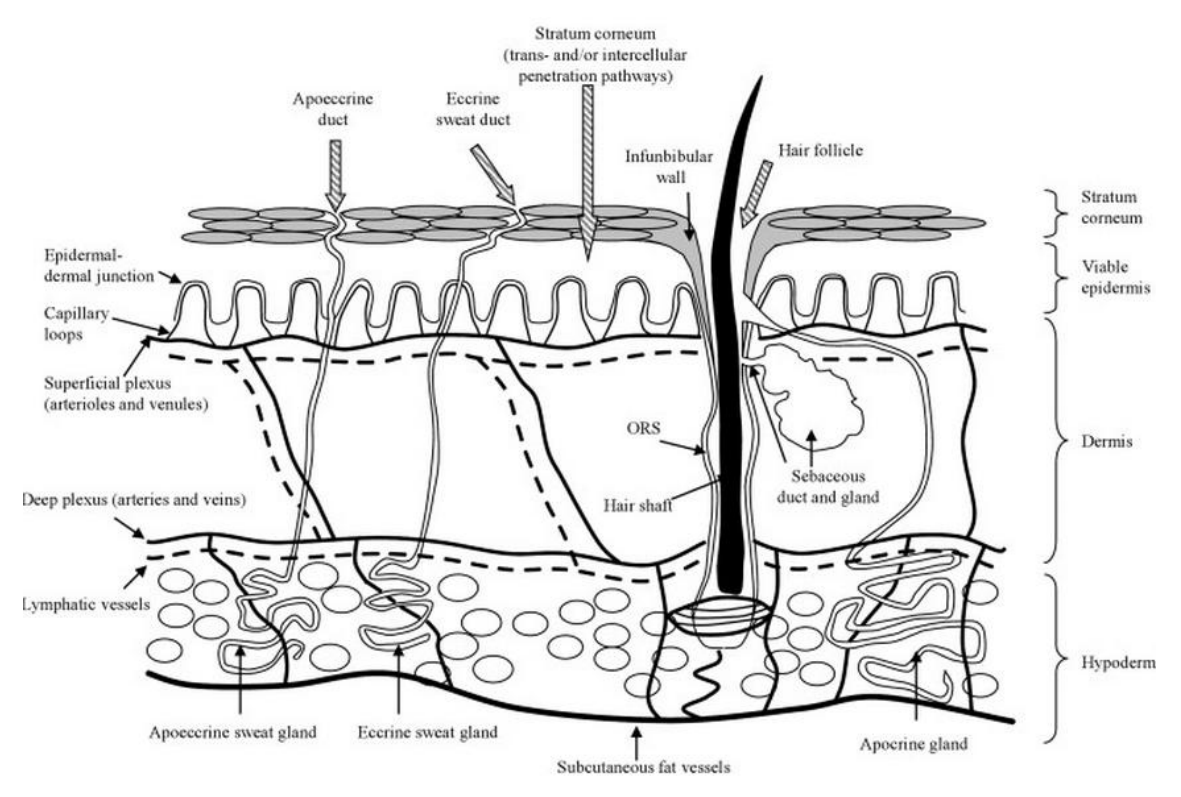


**Figure 1.1.** A schematic view of the human skin (adopted from *Advanced Drug Delivery Reviews*, vol. 65, pp. 152-168, 2013 [8]).

# 1.3. General design of transdermal patch

General designs of market-existing patch can be classified as shown in Figure 1.2. In reservoir system, backing membrane provides mechanical support and flexibility as well as prevents drug reservoir from dehydration. Amount of drug available to the skin is controlled by a membrane right under the drug reservoir. In matrix system, adhesive layer serves as a drug capacity to store drug in addition to its attachment function. A

rate-controlling membrane controls the amount of drug passing through via diffusion.

Unfortunately, the effectiveness of transdermal delivery by these designs is severely hampered by drug permeability across the lipoidal barrier of the stratum corneum.

Gradient dependence of drug diffusion mechanism further lowers drug availability at the later stage of delivery.

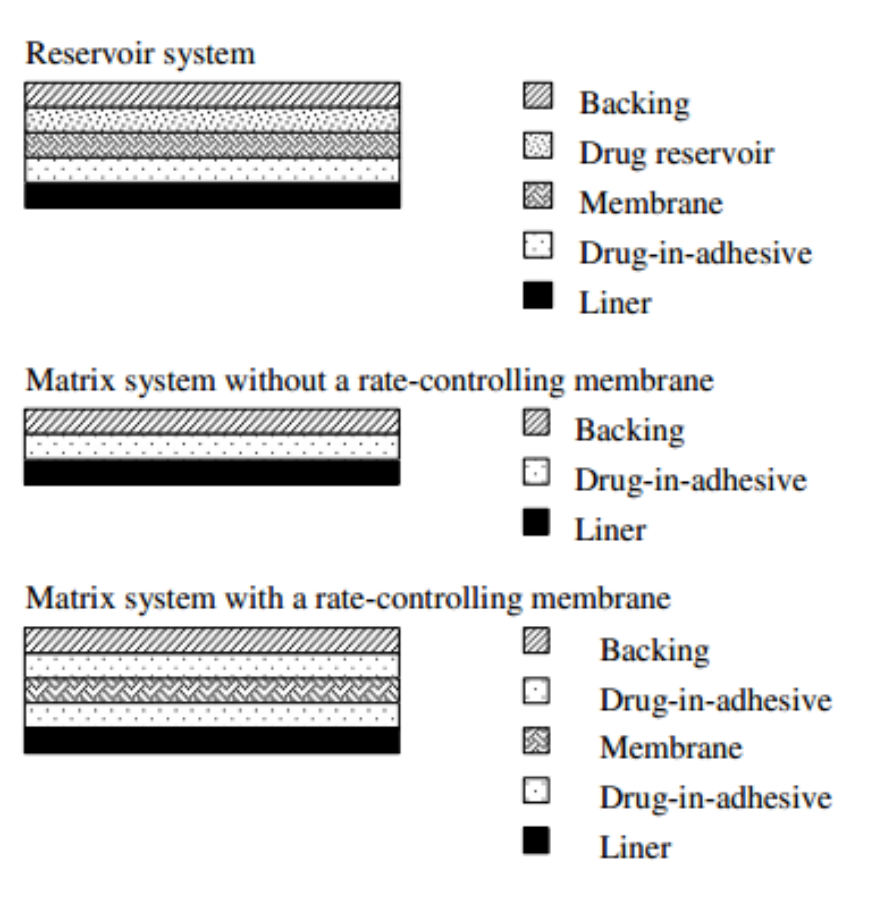


**Figure 1.2.** Generalized designs of conventional transdermal patch (adopted from *European Journal of Pharmaceutics and Biopharmaceutics*, vol. 64, pp. 1-8, 2006 [9]).

#### 1.4. Challenges in current transdermal patch design

All drugs presently administered across the skin share three constraining characteristics: low molecular mass (< 500 Da), high lipophilicity (oil soluble), and small required dosage (up to milligrams). These characteristics can be explained by the equation of steady state diffusion. After time t, the rate of diffusion approaches equilibrium and the steady state flux  $(\frac{d_m}{d_t})$  becomes:

$$\frac{\mathrm{d}_m}{\mathrm{d}_t} = \frac{DC_0K}{h}$$

**Equation 1.1.** Steady state flux at equilibrium (adopted from *European Journal of Pharmaceutical Sciences*, vol. 14, pp. 101-114, 2001 [10]).

where m is the cumulative mass of drugs diffused to receptor per unit area, D is the diffusion coefficient,  $C_o$  is the concentration of drug in donor at equilibrium, K is the partition coefficient of drug between receptor and membrane (skin), and h is the membrane thickness [10].

Based on the above equation, for optimal drug diffusion, the drug should feature low molecular weight (higher D), high lipophilicity (higher  $C_o$ ), and high partition coefficient. From the physiological point of view, tight cellular junction of the stratum corneum only allows small-sized drug to pass through. Lipid bilayer structure of dead

keratinocytes membrane favors oil soluble drug to pass through. Higher concentration difference between membrane and receptor provides stronger driving force for solute diffusion. Many drugs (e.g., DNA and hormones), however, possess characteristics that are not favorable (i.e., bulky and very water soluble) to be delivered in the transdermal route. For that reason, there is a strong need to develop different approaches that can improve drug permeation across the skin.

# 1.5. Approaches in overcoming the barrier

#### 1.5.1. Drug delivery by passive means

Market-existing approaches target the breakage of the stratum corneum which is the major barrier of topical drug delivery by mechanical or chemical means. Mechanical removal of the uppermost layer, so-called skin abrasion, eliminates possible drug blocking by the uppermost layer of the skin and hence improves the drug permeation during transdermal medication. Skin abrasion relies on the dermatological technique that is commonly used in superficial skin polishing—microdermabrasion for scars and other

skin imperfection treatment [11]. Similarly, microscissuining utilizes rubbing of the outer skin with micron-sized metal granules to erode the impermeable layer, providing microchannels for drug diffusion. The major advantage of skin abrasion is that the delivery is not restricted by physicochemical properties of potential drug to be delivered. Wu et al. demonstrated 20-fold improvement in drug diffusion across abraded skin using fluorescently-labeled dextran compared to that across intact skin [12]. Lee et al. reported that the application of microdermabrasion for 3 seconds led to 25-fold higher flux of hydrophilic vitamin C through the treated skin [13]. The effectiveness of multiple drug delivery has already been illustrated in case of biopharmaceuticals and vaccines [14]. Skin abrasion is necessary every time before medication due to the regeneration of the stratum corneum. Repeated removal of the stratum corneum, however, is susceptible to allergies and other infectious diseases because of the loss of the protection layer, limiting the long-term use of skin abrasion.

Chemical means, in contrast, reserves an ability to restore barrier's properties. The chemical reagents for increasing permeability of the superficial layer are known as chemical penetration enhancers. These enhancers partition into and interact with the

stratum corneum, and suppress its barrier's properties without further disrupting cells underneath. The suppression is reversible, i.e., only temporary disruption of the blocking properties. Different chemical enhancers act by different mechanisms, but generally they exert direct effects to the stratum corneum by: denaturation of the stratum corneum component and thus increasing skin hydration and diffusion permeability; modification of lipid domain embedded in lipid bilayers to reduce permeant resistance in the stratum corneum; or change in skin's solvent nature so that the drug or co-solvent partition into it. Various chemicals are suitable for playing the roles of chemical enhancers: azone is capable of increasing 5-fluorouracil flux across epidermal membranes by approximately 100-fold [15]; pyrrolidones can dramatically improve transdermal flux of mannitol by 200-400-fold [16]. Other naturally occurring resources such as fatty acids, urea, and phospholipids are also potential candidates for this particular purpose [17]. Unfortunately, selection of a unique penetration enhancer for a set of given permeants is still impossible because of the difference in physicochemical properties. The complex concentration effect of most enhancers further complicates the dosage control as well as steady drug release.

#### 1.5.1.1. Microneedles

Apart from chemically modifying skin structure to improve solutes' permeability towards the skin, researchers have focused on mechanical breakage of the rate-limiting barrier while inducing minimal or harmless immune response. Thanks to the advanced technology of microfabrication, synthesis of needles in micron size (100–1,500 µm) can be achieved in the past decade. The first microneedles intended for drug delivery were synthesized by photolithography and ion etching on silicon wafers [18]. More recently, other production processes involving metal, polymer, and sugar have been investigated to produce microneedles of lower cost but more biocompatible [19-21].

Short microneedles (i.e., 100–800 µm) could not reach the sensory cell embedded in the dermis layer, thereby allowing painless microneedle piercing to patients. The piercing is also capable of stimulating Langerhan cells in the epidermis to transform into active antigen presenting cells, offering microneedle competitive advantages over clinical needle in vaccine usage. Researchers have demonstrated improved immunogenicity and complete protection by using vaccine-coated microneedle against influenza virus in mice [22].

Microneedles can be generally categorized by their shape. Solid microneedles are closed-tip microneedles aiming to generate fissures to enhance drug diffusion. After the application of solid microneedles, they are removed from the skin and patch containing drug formulation is adhered to the site of microneedles application so that the drug in patch can pass through the microchannels created by the microneedles. Although improved drug permeability has been reported [23, 24], bioavailability of the drug was inconsistent due to passive transport phenomenon. Other determining factor involves the resealing ability of the microchannels, with fast closing of the channel blocks drug passage while long opening exposes the ease of infection [25]. Researchers therefore put emphasis on coating drug on solid microneedles. A wide range of drugs including low molecular weight drugs, DNA, proteins, and dysfunctional pathogens were proven to be effectively coated on microneedles [26]. This approach however poses a drawback that only small quantities of drugs can be coated as increased coating thickness diminishes delivery efficiency [27].

Unlike solid microneedles, hollow microneedles permit pressure-driven flow and hence larger flux into systemic circulation. The concentration-independent drug

permeation enables easy dose control based on patients' need. Aside from passive diffusion [28], it is possible to actively deliver drug solution through the microneedle bore by syringes, micropumps on microfluidic chips, bubble formation, finger pressure force, etc. [29-32]. Because of its high compatibility with other drug driving technologies, it is a promising way to incorporate hollow microneedles with other systems to further improve the bioavailability of drug, which will be described in Section 1.5.3.

Lately, dissolving microneedles have been fabricated by molding polymer or sugar mixture together with drug formulation into micromolding masters. When the microneedles are applied through the skin, the encapsulated drug is continuously released into deeper tissues upon polymer/sugar degradation/dissolution. The release rate can be controlled from minutes to months by the choice of polymer/sugar, depending on its proposed application [33]. For example, microneedles made with carboxymethylcellulose and amylopectin showed complete dissolution of the microneedles and release of encapsulated protein in 1 hour [34]. The key advantage of using dissolving microneedles is the elimination of medical hazardous sharp waste as

the entire microneedles would be degraded and absorbed by the skin ultimately. The encapsulation method may, however, make it more vulnerable to drug activity loss due to involvement of different solvents and high temperature in certain cases. The low drug loading capacity in consideration of the mechanical strength of microneedles also limits their broad applications.

# 1.5.2. Drug delivery by active means

The dependence of delivery rate on solute's concentration gradient in passive delivery has its own drawbacks as discussed in Section 1.5.1. Considerable effort has been taken to explore innovative ways of delivery. In what follows, recent attempts in active drug delivery will be discussed.

# 1.5.2.1. Iontophoresis

Iontophoresis is a non-invasive yet active transport measure to propel high concentration of charged drug molecules into deeper skin layer by repulsive

electromotive force. The rate of delivery heavily relies on current intensity and characteristics of solutes to be delivered [35]. Facilitation of the drug delivery can be explained by three phenomena: iontophoresis forces drugs with same charges through the skin by electrostatic repulsion; small current applied on the effective diffusion area lowers the skin's protective barrier function; and water passes through the stratum corneum by electroosmosis, carrying dissolved solutes across the layer [36]. A number of anti-inflammatory drugs and analgesics were tested and showed higher transdermal delivery efficiencies with iontophoresis [37-39]. Its application is however hindered by the size of solutes (< 500 Da). Larger molecules such as insulin cannot be transported by iontophoresis solely.

# 1.5.3. Combined use of the technologies

There is high possibility of combining different delivery mechanisms to achieve better performance. Chen et al. tested and evaluated the synergetic effect of liposome (chemical enhancer), iontophoresis, and solid microneedles towards the delivery of insulin both in vitro and in vivo [40]. Liposome helps protecting insulin from

environmental shocks and increasing insulin permeation, iontophoresis plays its role in carrying charged insulin encapsulated liposome to the receptor, and solid microneedles generate fissures to bypass the rate-limiting barrier. It was reported that in case of the same formulation of nanovesicles carrying insulin into the circulation system, iontophoresis increased the permeation rate of insulin by more than 4-fold when compared with nanovesicles alone, while insulin-encapsulated nanovesicles delivered through solid microneedles-made fissures showed 100-fold enhancement. The combined use of nanovesicles, iontophoresis, and solid microneedles improved the permeation rate by 300-fold. The results illustrate that microneedles play a significant role in microporation especially when the delivery is hindered by the characteristics of drugs (i.e., molecular size, polarity, and lipophilicity).

Qin et al. further developed a basal and on-demand bolus insulin delivery system to manage diabetic mellitus properly [41]. The system was composed of short microneedle and iontophoresis patch. By controlling the current intensity and "on-and-off" (pulse duration) of the iontophoresis patch on microneedle-treated skin, the system presented therapeutic equivalence to insulin pump with long- and short-acting insulin to meet

on-demand dose. Yet, the incorporation of iontophoresis with microneedles may be at high risk of irritation because of the high constant localized current to area with low impedance (i.e., microneedle-treated skin) [42]. It is therefore desirable to develop a relatively safe medical device that can accurately deliver drug in a time-controlled manner.

#### 1.6. Continuous drug delivery

Recently, continuous drug delivery has drawn considerable attention over conventional short-term single-dose delivery. In fact, the advantages of continuous drug delivery have been clearly indicated by many researchers. Stockwell and colleagues showed that dyskinesia level, a motor complication, of Parkinson's disease patients having continuous subcutaneous delivery of ropinirole was lower than that of patients having twice daily oral administration [43]. In Sloan and colleagues' clinical study, 63% of cancer patients preferred the use of transdermal delivery of fentanyl administered every 3 days over chronic oral morphine analgesia for pain killing [44]. For patients suffering from diabetes mellitus (DM), continuous delivery of human insulin

(short-acting/regular) could be better than single-dose delivery of insulin analogues (long-acting) as studies revealed that the injection of insulin analogues may lead to unexpected outcome [45]. A more recent study stated a questionable view towards the risk for breast cancer associated with the use of insulin glargine [46]. In short, continuous drug delivery has offered considerable advantages over single-dose/bolus therapy in different biomedical applications. Designing a continuous delivery patch that can be loaded with diverse drugs gives rise to a large market potential and great convenience.

## 1.6.1. Delivery of insulin: a case study

Glucose plays its significant role as a primary source of energy to cell metabolism in body for normal daily activities. Its concentration in blood is tightly regulated by homeostasis as too high (hyperglycemia) or too low (hypoglycemia) blood glucose level may result in mild to serious issues such as unconsciousness, poor wound healing, and permanent damage to the neurological system. The regulation is dominated by insulin, through controlling the activity of cell membrane-embedded transporter protein that

allows glucose flux in and out from cells. Insulin is also responsible for the control of glucose–glucagon conversion for carbohydrate storage in the liver and muscle cells.

DM can be regarded as a group of diseases with hyperglycemic symptoms caused by the influence of insulin. This influence could be contributed by, in general, malfunction of insulin-producing beta cells of the islets of Langerhans (type 1), or insensitive insulin detection by insulin receptor with lower insulin secretion coupled in some cases (type 2). DM patients can be characterized by a fasting glucose level of higher than 7.0 mM. All DM type 1 patients and some type 2 patients with declining beta cells' function should be given insulin treatment. For a healthy subject, the insulin levels in response to high carbohydrate or protein meals can be generally summarized in Figure 1.3.

The breakdown of carbohydrate in meals leads to the rise of blood glucose level, triggering the responsive insulin release to blood for regulating blood glucose concentration. The insulin level drops to basal progressively through self-regulation as glucose is steadily taken up by cells. Basal level is necessary for maintaining essential metabolisms in body.

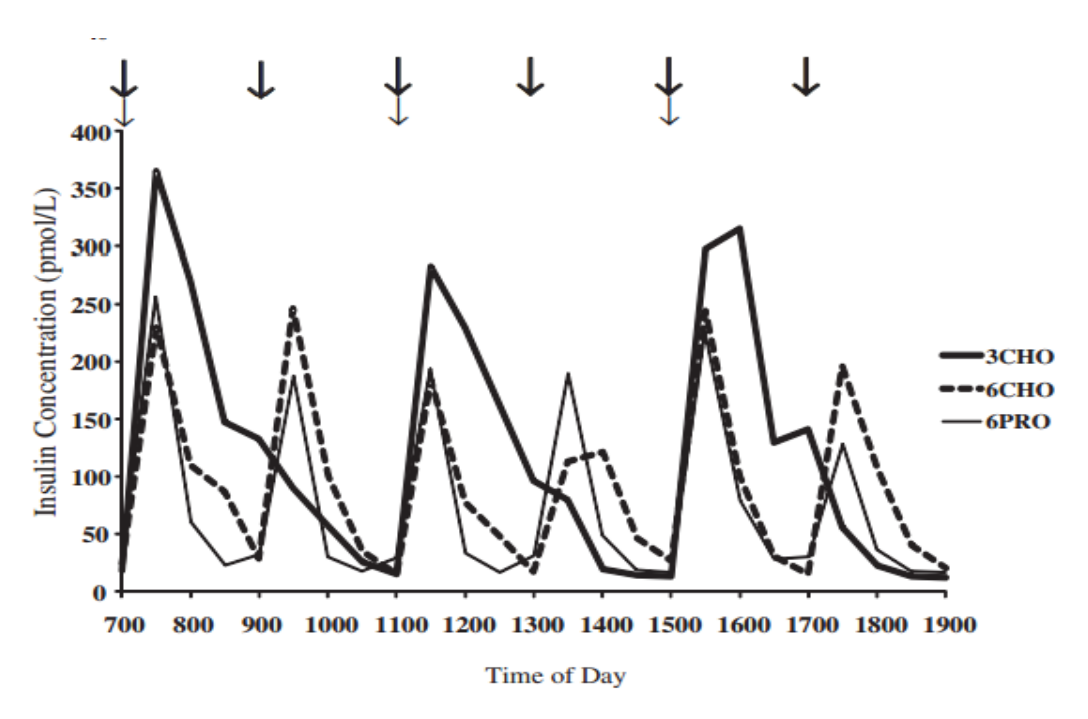


**Figure 1.3.** Normal insulin responses to three high carbohydrate (3CHO), six high carbohydrate (6CHO), and six high protein (6PRO) meals daily (adopted from *The European e-journal of Clinical Nutrition and Metabolism*, vol. 5, pp. 277-280, 2010 [54]).

In current therapeutic strategies, patients are advised to use either a single type or combined mixture of different types of insulin according to their respective pharmacokinetics [47, 48]. Pharmacokinetics refers to the study of absorption, distribution, and elimination of the administered drug. Figure 1.4 lists some insulin forms and their corresponding pharmacokinetics by intravenous injection. Insulin analogues can be mainly categorized as short-acting and long-acting. Short-acting

insulin provides maximum pharmaceutical effect 1–2 hours after administration and diminishes in 4–6 hours while long-acting insulin gives no pronounced peak and can last up to 24 hours [49]. Short-acting insulin is usually injected before each meal to minimize blood glucose level fluctuation while long-acting insulin is given once or twice a day to simulate the normal basal insulin level. As mentioned in Section 1.6, there exists potential cancer risk associated with the use of insulin analogues.

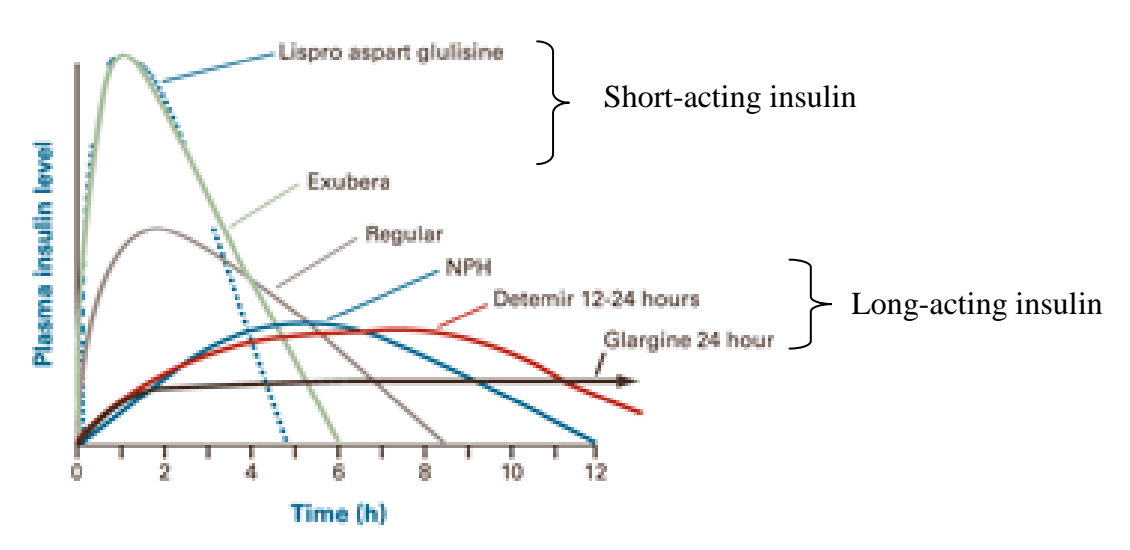


**Figure 1.4.** Pharmacokinetics of different insulin analogues in human (adopted from *American Journal of Management Care*, vol. 13 Supplement 2, pp. 47-54, 2007 [55]).

Despite the limited usage of human insulin due to its pharmacokinetics, the administration of human insulin permits an alternative and desirable way in insulin

therapy for DM patients. The major challenge of human insulin application is its intermediate-acting character: giving less marked peak 2 hours after injection compared to short-acting insulin and retaining its effect until slightly more than 8 hours after administration. For this reason, tight blood glucose level control is difficult. The high glucose variation has been reported to provide adverse effects such as cardiovascular diseases and retinopathy [50, 51]. On the contrary, continuous delivery of human insulin prevents DM patients from these complications, and the fabrication of a patch featuring continuous delivery of insulin would be highly favorable.

It is important to determine the dimensions of patch based on patients' needs. For example, the average body weight of male is 62 kg [52]. Given that:

Total daily insulin requirement =  $0.55 \times \text{total}$  weight in kilograms

**Equation 1.2.** Daily insulin dose of a DM patient (adopted from http://dtc.ucsf.edu/types-of-diabetes/type2/treatment-of-type-2-diabetes/medications-an d-therapies/type-2-insulin-rx/calculating-insulin-dose/#formulas [53]).

A 62 kg patient requires  $0.55 \times 62 \approx 34$  IU/day. Half of the dose (17 IU/day) is for bolus therapy given before each meal, and the remaining half is for basal therapy. Assuming each basal therapy patch is used for 8 hours, it should contain 5.67 IU insulin.

Market-existing insulin is supplied at a concentration of 100 IU/mL. Take the dead

volume of the patch to be 20%, the capacity of drug reservoir should be at least 70  $\mu$ L. The dimensions of the transdermal delivery patch that will be described in Section 2.2.5 are determined based on the above calculations.

#### 1.6.2. Active infusion

Most of the transdermal systems are driven by passive infusion (i.e., drug delivery through the barrier by diffusion), which may not be applicable when constant and sustained drug release is required. The non-steady rate is the result of concentration dependence of the transport phenomenon. Active infusion, forcing drug-containing liquid out to tissues by mechanical means, is thereby a preferred drug delivery approach since the driving force is independent of solute's concentration. Indeed, studies have shown active infusion with microneedles was feasible, which was discussed in Section 1.5.1.1 [56]. McAllister and colleagues demonstrated insulin delivery by means of microneedles and pressure force (10 psi), lowering blood glucose level by 70% [57].

Lately, a regulated drug delivery was achieved by manipulating a thin-film heater on a printed circuit board to control heat applied to a thermo-expandable composite

(Figure 1.5), which consisted of low boiling point volatile organic compound (VOC) entrapped by thermoplastics with low glass transition temperature [58]. The composite expanded in volume when heated. Expansion of the composite would force insulin out from the drug reservoir through the open-tube microneedle array. Precise control of insulin release from the device could significantly lower blood glucose level (50% reduction 3-hour post-delivery). Involvement of the use of battery, however, hampers the portable usage of the device.

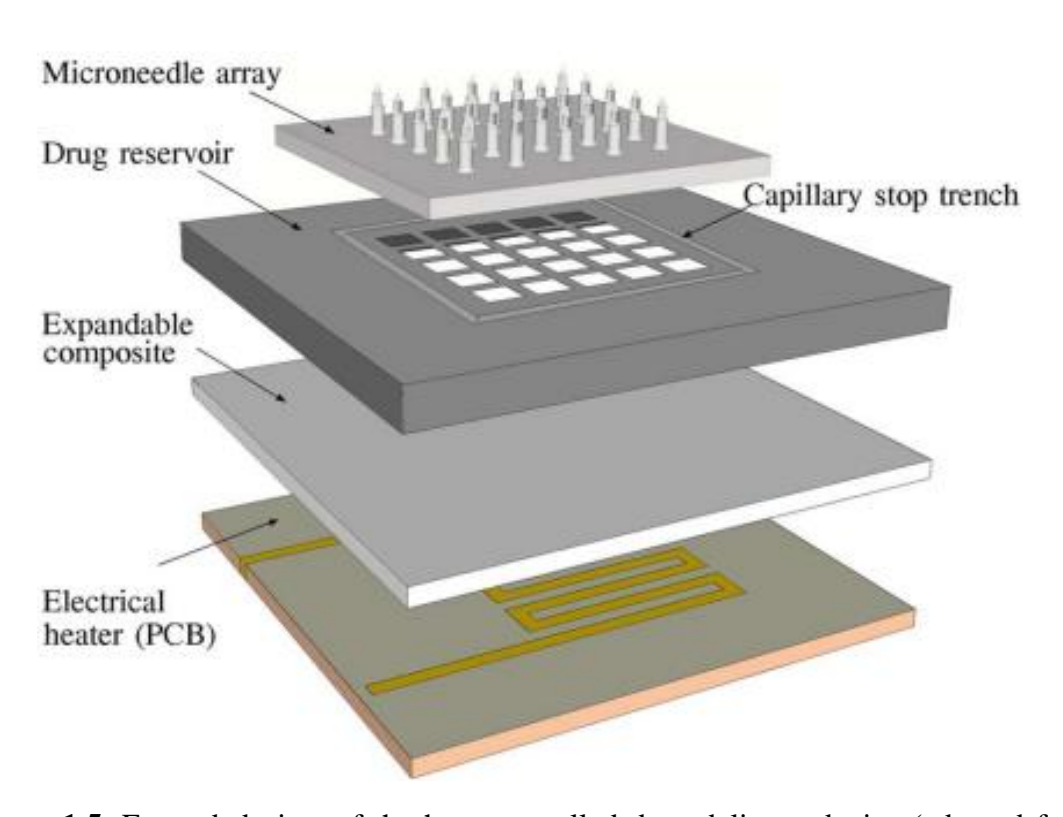
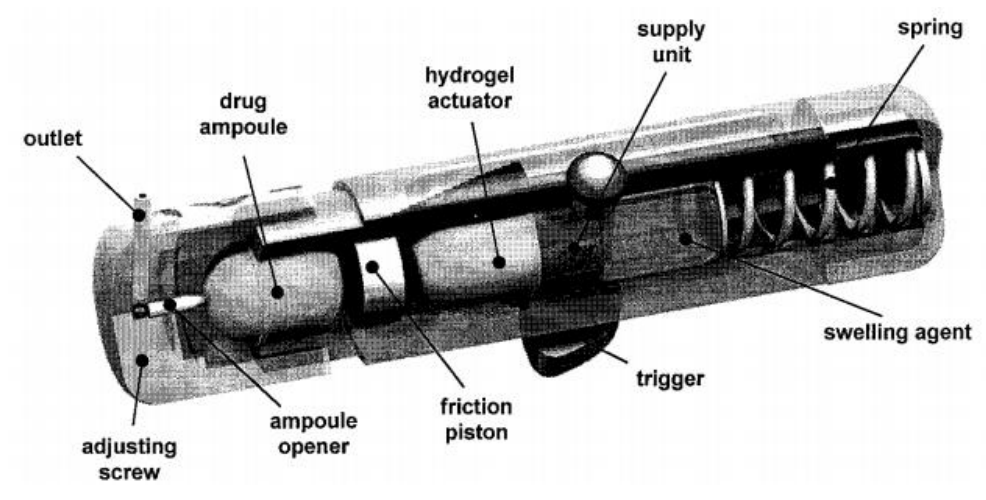


Figure 1.5. Expanded view of the heat-controlled drug delivery device (adopted from

*IEEE Transactions on Biomedical Engineering*, vol. 55, pp. 1063-1071, 2008 [58]).

On the other hand, an autonomous pump was designed for treating Dawn phenomenon of diabetic patients (Figure 1.6). The pump made use of swelling force of pH-dependent hydrogel to trigger drug release. An adjustable counter force provided by a friction piston was designed to achieve controlled-release with time delay. As a result, the pump showed zero-order release delivering 300 µL of drug in 6 hours [59]. The pump, however, is too bulky to be portable for daily use. The ease of sterilization of the drug ampoule in the device is another concern. The development of a small, disposable, and safe transdermal patch with sustained and steady drug delivery is therefore highly desirable.



**Figure 1.6.** A drug delivery device with an autonomous pump (adopted from *Macromolecular Symposia*, vol. 210, pp. 377-384, 2004 [59]).

### 1.7. Hydrogel

Hydrogel is regarded as a three-dimensional network of hydrophilic polymer that can absorb large amount (up to 99.9% of its dried weight) of water for volume expansion without changing its structural orientation. The first study of hydrogel in biological application was reported by Wichterle and Lim in 1960 [60]. Swelling ability, phase transition, choice of solvent, and environmental stimulus have been extensively studied since 1968 [61]. The ability of water absorption in hydrogel is attributed to the hydrophilic domains in the polymer network such as the presence of hydroxyl, sulfo, carboxyl, or amide group. Hydrogel can be categorized by morphological structure hydrogen-bonded, semi-crystalline, and supramolecular), way crosslinking (physical and chemical), degree of stimulus response (stimulus-sensitive and -insensitive), type of charge (neutral and ionic), or origin (synthetic, natural, and combinational). The swelling performance and characteristics of hydrogel could be controlled by various parameters, which include monomer type, initialization system of polymerization, choice of crosslinker, conjugate, and polymerization method [62].

### 1.7.1. Theoretical swelling studies

It is essential to investigate the correlation of parameters that control the swelling equilibrium as well as the dimensional change in order to predict and design hydrogel for intended purpose. The swelling kinetics influence the time needed for the uptake of swelling agent and substances dissolved in swelling agent by hydrogel. It is of particular interest to study the swelling kinetics in case of actuator as its application is based on the swelling ability. Hence, considerable efforts have been devoted to mathematical modelling of swelling phenomenon and predictability of hydrogel's characteristics in the past decades [63, 64].

In general, once swelling agent contacts with a non-swollen hydrogel, the solutes in the agent interact with hydrogel surface and penetrate into the polymer mesh. The outer solvated rubbery phase is distinguished from the inner unsolvated glassy phase of hydrogel by a moving boundary. Expansion of the polymer network in the rubbery phase increases the mesh size, allowing higher solute flux to the glassy phase. Hydrogel swelling ratio is contributed by two factors. The main driving force is osmotic swelling force that determines its solvent adsorption as well as volumetric change. A counter

elasticity force helps restricting the swelling force to prevent morphological deformation.

When the two forces are balanced, the swelling is in equilibrium and no further swelling occurs [65].

The water driving force also depends on the pore size and its distribution in hydrogel system. A power law equation was established to govern the water diffusion into the network:

$$\frac{W_t}{W_{\infty}} = kt^n$$

**Equation 1.3.** Power law equation (adopted from *Journal of Controlled Release*, vol. 5, pp.23-26, 1987 [66]).

where  $W_t$  and  $W_\infty$  are the weight of hydrogel at time t and equilibrium respectively, k is the characteristic constant related to the solvent–polymer interaction. The transport number, n, depends on the size and geometry of the network available for solute exchange or uptake. The type of transport within the system can be determined according to the value of n given in Table 1.

Fickian diffusion occurs when the solvent diffusion rate is lower than the polymer relaxation rate in case of one-dimensional geometry or small-volume swelling, while

non-Fickian case II transport is dominated when the rate of diffusion outweighs the structural relaxation rate. The anomalous transport is controlled by both diffusion and relaxation when these two factors are comparable.

**Table 1.** Fickian diffusion models and their time dependence.

Value of n	Type of transport	Time dependence
= 0.5	Fickian diffusion (case I)	t 1/2
0.5 < n < 0.1	Non-Fickian diffusion (anomalous transport)	t <sup>n-1</sup>
= 1	Non-Fickian diffusion (case II)	independent

# 1.7.2. General applications

Thanks to its high biocompatibility, hydrogel has been widely used as drug carrier. For example, Zhang and colleagues modified the microstructure of hydrogel to improve drug release performance by the formation of microgels as primary structure and cross-linking of the microgels into bulk network as secondary structure [67]. The release yield of drugs from the modified hydrogel was 4 times higher than that of the conventional one. In addition, modification of hydrogel end group could also alter its stimuli-response behavior. Gu and colleagues demonstrated that the incorporation of

carboxyl groups into poly(N-isopropylacrylamide) matrix led to dual response to both pH and temperature [68]. The dual-responsive hydrogel showed almost complete release of isoniazid into gastric acid-mimicking medium. Besides, due to the diverse characteristics of hydrogel, it has been extensively studied for various uses. For instance, Kumar and co-workers reported the use of pH-responsive hydrogel for oral insulin administration [69]. In lab-on-a-chip field, a self-actuated thermo-responsive hydrogel valve was developed in 2005 [70]. The outstanding swelling property of hydrogel is a good candidate to be an actuator in the drug delivery system.

## 1.7.3. Applications as actuators

The reversible swelling—shrinking property of hydrogel is well utilized in microsystem research. The self-sensing and -response functionalities offer automatic characteristics that have not yet been found in other materials or systems. The controlled and repeatable swelling—deswelling steps allow the generation of fluidic propulsion. Eddington et al. fabricated a pressure-driven microdispensing device as shown in Figure 1.7 [71]. Poly(acrylic acid-2-hydroxyethyl methacrylate) copolymer was

photocrosslinked in chambers by selective exposure of pre-cured mixture under UV. The pH-sensitive hydrogel expanded in alkaline and contracted in acidic medium. Swelling agents for valve and actuators were fed into separated reservoirs to allow individual control. Expansion of hydrogel in valve led to valve closure that prevented leakage of fluid to be delivered and allowed buildup of propulsion pressure. The micropatterning of hydrogel actuators facilitated rapid response towards external stimulus. The infusion rate could be increased up to 540 µL/min with the relaxed valve.

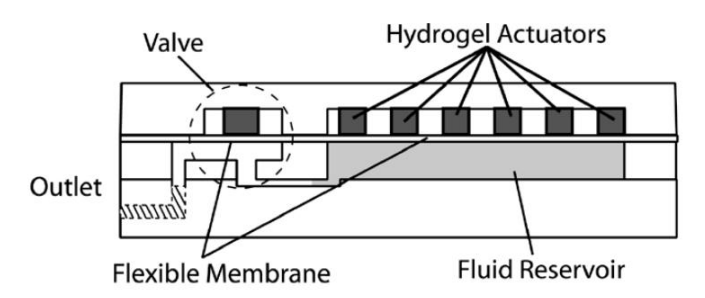


**Figure 1.7.** A microdispensing device driven by a pressure pump (adopted from *Macromolecular Symposia*, vol. 210, pp. 377-384, 2004 [71]).

Aside from pump, another potential application of hydrogel would be artificial muscle. Ismail's group incorporated the unique properties of two polymers to form hybrid microfiber [72]. Biocompatible and pH-stable chitosan matrix was embedded

into electroconducting polypyrrole. Upon oxidation, anions and solutes rushed into the hybrid matrix, resulting in actuation.

In short, the unique biocompatibility and swelling ability of hydrogel have enabled many different applications. It is very likely that its actuation ability can be utilized for achieving steady and sustained transdermal drug delivery.

### 1.8. Objectives of the study

The main objective of this study is to develop a continuous transdermal drug delivery patch featuring painless and non-allergic drug delivery through the skin using hollow microneedles.

One important task is to achieve steady and sustained drug delivery (i.e., 8 hours), which is accomplished by controlling the swelling rate of hydrogel actuator. For basal insulin delivery in diabetes management, the proposed drug release rate would be 7.1  $\mu$ L/h of 100 IU/mL insulin solution for a 62-kg patient.

Another task is to apply the developed transdermal delivery system on different medications including insulin and diclofenac sodium (DFS).

Yet another task is to ensure that the transdermal patch to be portable (i.e., small size) and disposable (i.e., low cost and easy-to-produce).

Last but not least, the pharmacodynamics of insulin delivered to diabetic rats using the developed patch is demonstrated.

# **Chapter 2**

# **Research Methodology**

# 2.1. Drug delivery scheme

A proposed transdermal microneedle patch is schematically illustrated in Figure 2.1. A dried hydrogel is placed above a reservoir where drug is loaded. An elastic membrane, which is chemically inert, is adhered between the hydrogel and drug reservoir to separate each other. The hydrogel reservoir is surrounded by a water reservoir to provide sufficient swelling agent (i.e., water). The swelling agent is added to the water reservoir through two resealable ports. The cap above the hydrogel and water reservoirs acts as a backing membrane to withstand swelling force from the hydrogel. A microneedle plate is sealed below the drug reservoir in order to facilitate transdermal delivery. In this design, a desired amount of drug solution is loaded into the drug reservoir by 31 G syringe needle through the resealable ports. After the addition of the swelling agent to the water reservoir, the patch is shaken gently to allow proper contact between the swelling agent and dried hydrogel. The dried hydrogel then swells in a time-controlled manner. Volume expansion of the hydrogel forces the elastic membrane down to the drug reservoir and hence the drug out through the hollow microneedles to the deep skin layer.

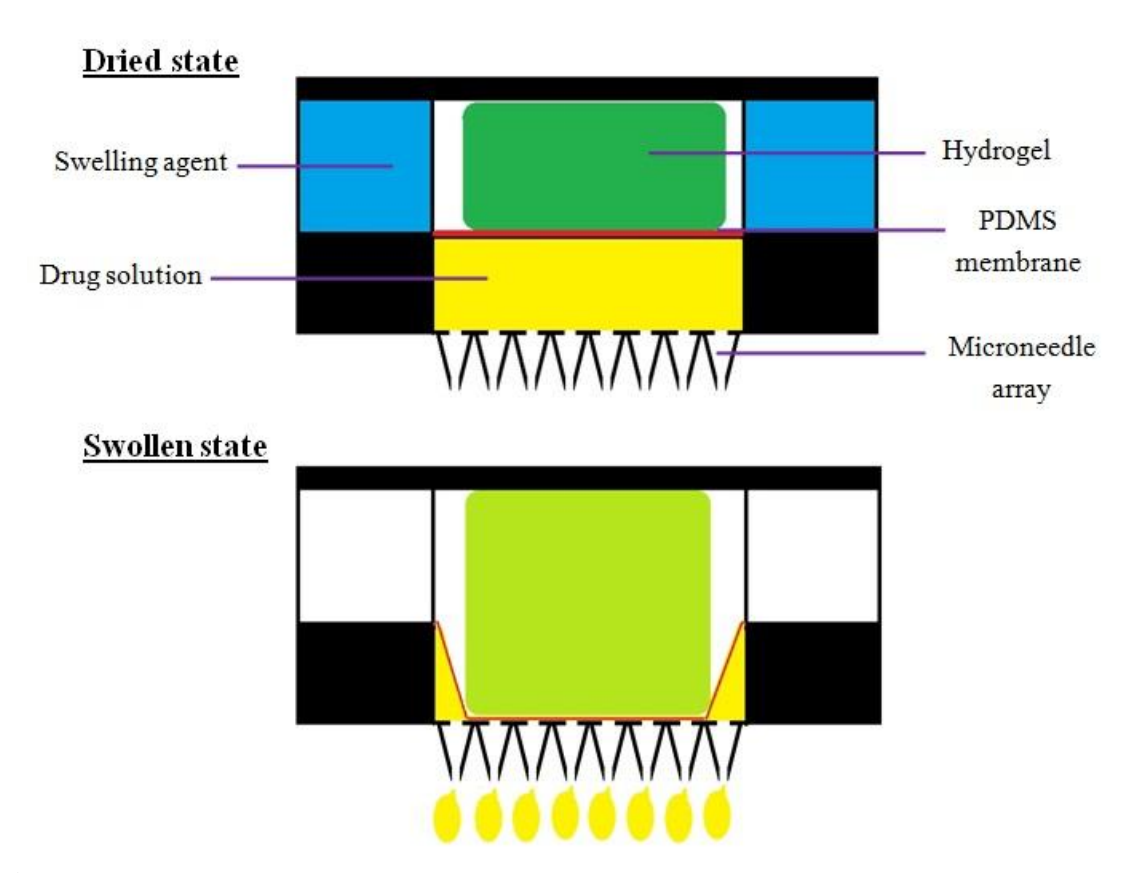


**Figure 2.1.** Delivery scheme of drug in the microneedle-adhered transdermal patch.

#### 2.2. Materials and methods

### 2.2.1. Materials and instrumentations

Acrylamide (AAm), ammonium persulfate (APS), N,N'-methylenebis(acrylamide) (MBAAm), polyethylene glycol with molecular mass of 4,000 g/mol (PEG4000), tetramethylethylenediamine (TEMED), hexane, sodium chloride (NaCl), potassium chloride (KCl), sodium dihydrogen phosphate heptahydrate (NaH<sub>2</sub>PO<sub>4</sub> 7H<sub>2</sub>O), potassium dihydrogen phosphate (KH<sub>2</sub>PO<sub>4</sub>), evans blue (EB), methylene blue (MB), diclofenac sodium (DFS), fluorescein-tagged insulin (FITC-insulin), trifluoroacetic acid (TFA), and acetonitrile (ACN) were purchased from Sigma-Aldrich. Absolute ethanol was obtained from UNI-Chem Chemical Reagents. Nitrogen gas (N<sub>2</sub>) was supplied by the Hong Kong Oxygen & Acetylene. Polydimethylsiloxane (PDMS) Sylgard 184 was purchased from Dow Corning. All solutions were prepared with deionized (DI) water (18.2 M $\Omega$  cm) from a Milli-Q Advantage A10 System (Millipore). Cyanoacrylate adhesive superglue and silicone conformal coating were obtained from RS Components. Expoxy gel was purchased from VersaChem. Silicone was purchased from local shop. Microscope glass slides (2" × 3") were purchased from Sail Brand. Double-coated

polyethylene tape (9766) was a kind gift from 3M. Silastic medical adhesive silicone type A was a free sample from Dow Corning. Close-tip AdminPatch® microneedle arrays (ME-C-600, 600 μm in length) were purchased from AdminMed. Open-tip zeolite microneedles grown on stainless steel plates (SSM-O-150, 150 μm in length) were obtained from the Department of Chemical and Biomolecular Engineering (CBME) at The Hong Kong University of Science and Technology (HKUST). Open-tip plastic microneedles (P-O-500, 500 μm in length) were obtained from the Department of Industrial and Systems Engineering (ISE) at The Hong Kong Polytechnic University (HKPU) [73].

In vitro drug delivery was tested in 7-mL capacity manual diffusion cell system (Hanson Research; Chatsworth, CA, USA). Rapid prototyping products were designed by SolidWorks (Dassault Systèmes SolidWorks Corporation; Waltham, MA, USA) and fabricated by Objet Connex 350<sup>TM</sup> 3-D printer with Objet FullCure720<sup>TM</sup> as raw material (Stratasys; Eden Prairie, MN, USA). UV–visible spectra were measured by an Ultrospec<sup>TM</sup> 2100 pro UV/visible spectrophotometer (GE Healthcare; Chalfont St Giles, UK). Visualization of hydrogel swelling was taken by Canon 40D body with EF-S 60/

F2.8 marco lens, Sea & Sea YS-110 strobes \* 2, TTL-controlled. Measurement of PDMS thickness on hydrogel was performed by field emission scanning electronic microscope, JSM-6300F (JEOL; Japan). DFS was quantified by the Acquity UPLC® system with photodiode array eλ detector and Acquity UPLC® BEH C<sub>18</sub> column, 130 Å, 1.7 μm, 2.1 mm × 50 mm (Waters; Milford, MA, USA). Fluorescence spectra were measured by SPECTRAFluor Plus (TECAN; Switzerland), connected to a computer (Magellan software). Blood glucose level of rats was measured by Accu-Chek® Performa Nano glucose monitor and test strips (Roche; Switzerland).

#### 2.2.2. Synthesis of polyacrylamide-co-polyethylene glycol

The hydrogel (PAAm-PEG4000) was synthesized by gently mixing 15 wt% AAm, 2 mL of 14 mM APS, 2.4 mol% MBAAm, and 9 wt% PEG4000 in 7 mL DI water [74]. The mixture was degassed with N<sub>2</sub> for 10 min. Then, 1 mL of 80 mM TEMED was added to the mixture with stirring. The mixture was rapidly poured into a plastic cylinder with inner diameter of 11 mm and was allowed to settle for polymerization. The open end of the cylinder was covered with parafilm 5 min after the start of reaction. The

cylinder was allowed to stay overnight for complete reaction. After that, the hydrogel was cut into smaller pieces, with the help of a spacer as shown in Figure 2.2. The width of the spacer was set to 3.6 mm (measured by an electronic calliper). The hydrogel was then washed with DI water for a week to remove unreacted substances with daily water replenishing. The hydrogel pieces were dried under vacuum for 2 days. The dried hydrogel had dimensions of  $6.47 \pm 0.03$  mm in diameter and  $1.7 \text{ mm} \pm 0.1$  mm in height.



Figure 2.2. Spacer for hydrogel cutting.

## 2.2.3. Spray coating of polydimethylsiloxane on hydrogel

The spray coating method is well described by Choonee and his colleagues [75].

In brief, PDMS was weighed and mixed with 10 w/w% curing agent to form a pre-cure mixture. Equal weight of hexane was added to the mixture to lower the viscosity. The mixture was then poured into a sprayer with a spraying pressure  $0.2 \text{ kgf/cm}^2$ , placing 0.3 m above the hydrogel (see Figure 2.3). The dried hydrogel was sprayed with the mixture for 10 s. After 2 min of settling, the hydrogel was heated in an oven at 80 C for 30 min. The procedures were repeated on the uncoated side of the hydrogel. The spray-coated hydrogel was stored in a desiccator until further treatment.



Figure 2.3. Polydimethylsiloxane (PDMS) spray coating setup.

#### 2.2.4. Synthesis of elastic polydimethylsiloxane membrane

PDMS was used as the raw material for the elastic membrane due to its high thermal and chemical stability as well as low elastic modulus. PDMS pre-cure mixture (10 w/w% curing agent) was poured on glass slides and degassed under vacuum for 30 min. The mixture was spun on glass slides at approximately 660 rpm for 1 min, followed by curing at 80 °C for 30 min to yield 140-µm thick membrane according to calculations [76]. Circular PDMS membranes of 16 mm diameter were cut and removed from the slides cautiously by forceps.

## 2.2.5. Design of the transdermal delivery patch

#### **First generation**

The first generation design was used in all in vitro tests because of its ease of mounting to the diffusion cell system (Figures 2.4–2.6). The assembly steps of the patch followed the general procedures in Section 2.2.6. The assembled patch had overall dimensions of 3.8 mm in height and 25 mm in diameter. The patch could hold up to 70 µL model drug, with swelling agent capacity of 400 µL.

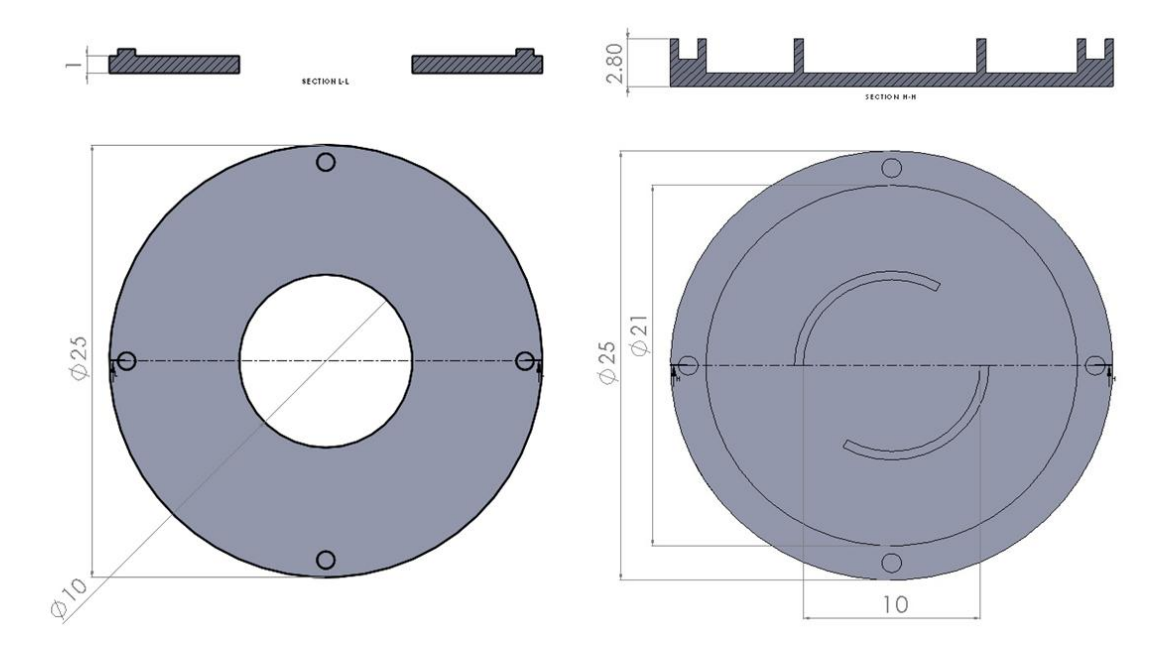


**Figure 2.4.** First generation - structures of (left) the insulin reservoir and (right) the water and hydrogel reservoirs showing their dimensions and alignment feature. (Top) Cross-sectional views across the dotted lines shown below and (bottom) surface views of the structures.

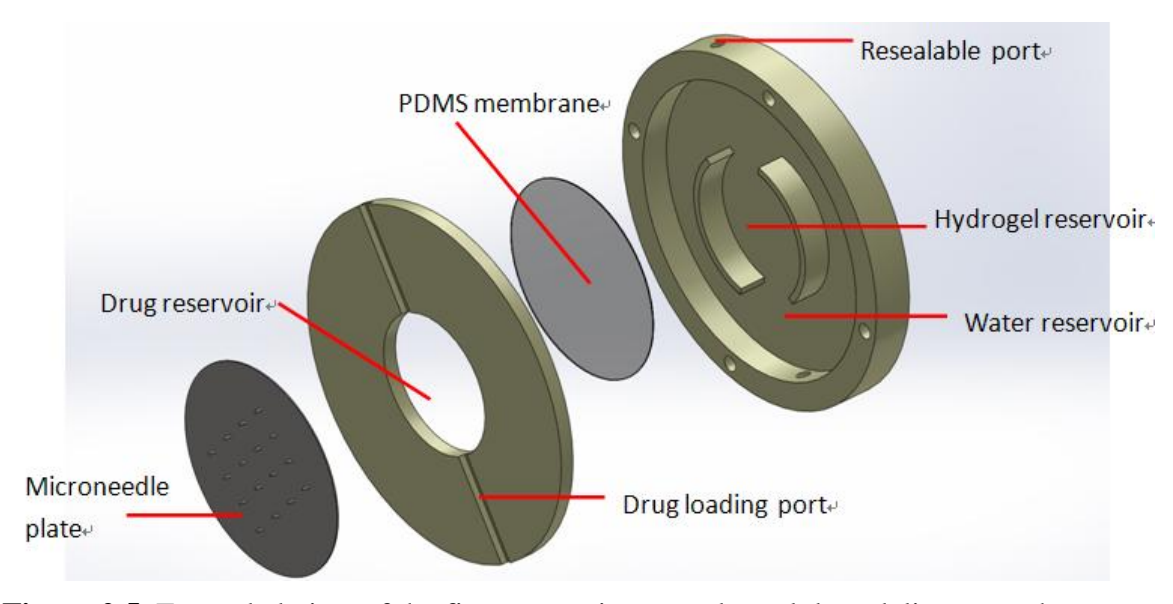


Figure 2.5. Expanded view of the first generation transdermal drug delivery patch.

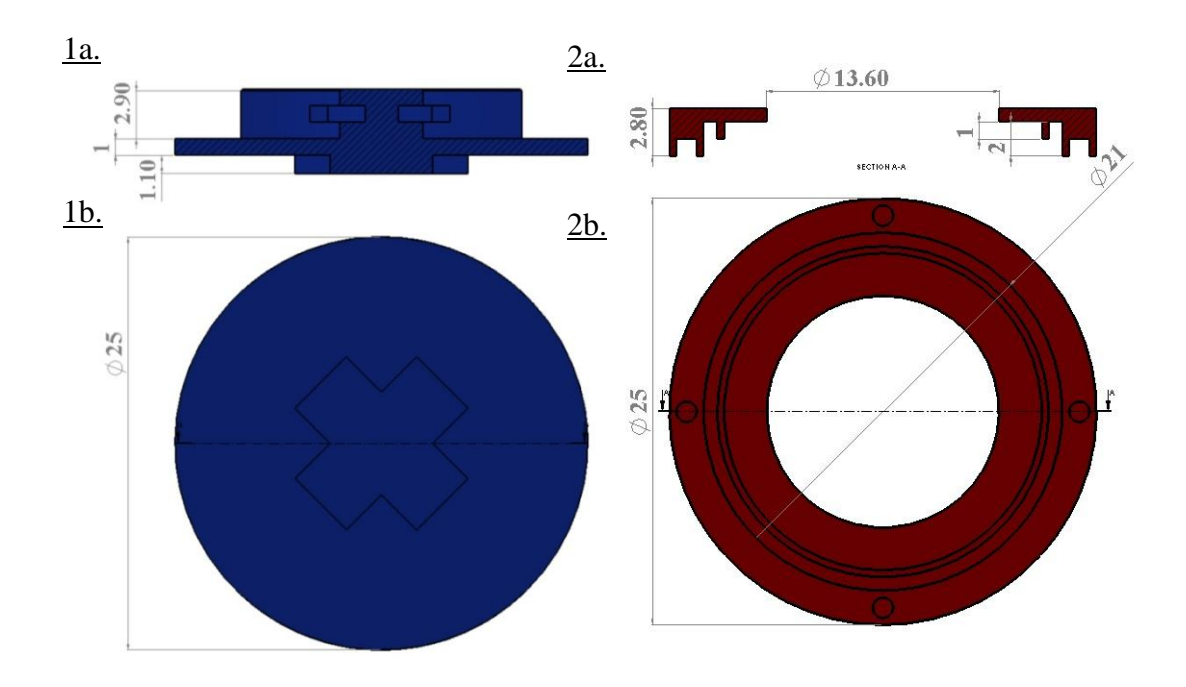


**Figure 2.6.** A prototype of the first generation assembled patch with zeolite microneedle (SSM-O-150).

#### **Second generation**

The second generation patch was modified from the first generation and used in all in vivo tests (Figures 2.7–2.9). It contained a detachable key that helps to trim the actual size of the patch down to 4 mm in height. The key–lock system could control gate opening and thus hydrogel swelling as well as drug delivery. The water blocking gates were built on a turnable cover. The junction between the water blocking gate and hydrogel reservoir would be sealed with epoxy resin to ensure complete isolation of swelling agent from hydrogel. The assembled patch could fit into a watch-like patch

holder with alignment points complementary to that of the backing cover, providing proper holding in axial and tangential direction. The lock of the turnable cover was exposed on the surface of the patch holder. Upon the turning of the water blocking gate, the swelling agent could get into the hydrogel reservoir once the complementary key is inserted. The assembled patch without the detachable key and patch holder had overall dimensions of 3.8 mm in height and 25 mm in diameter.



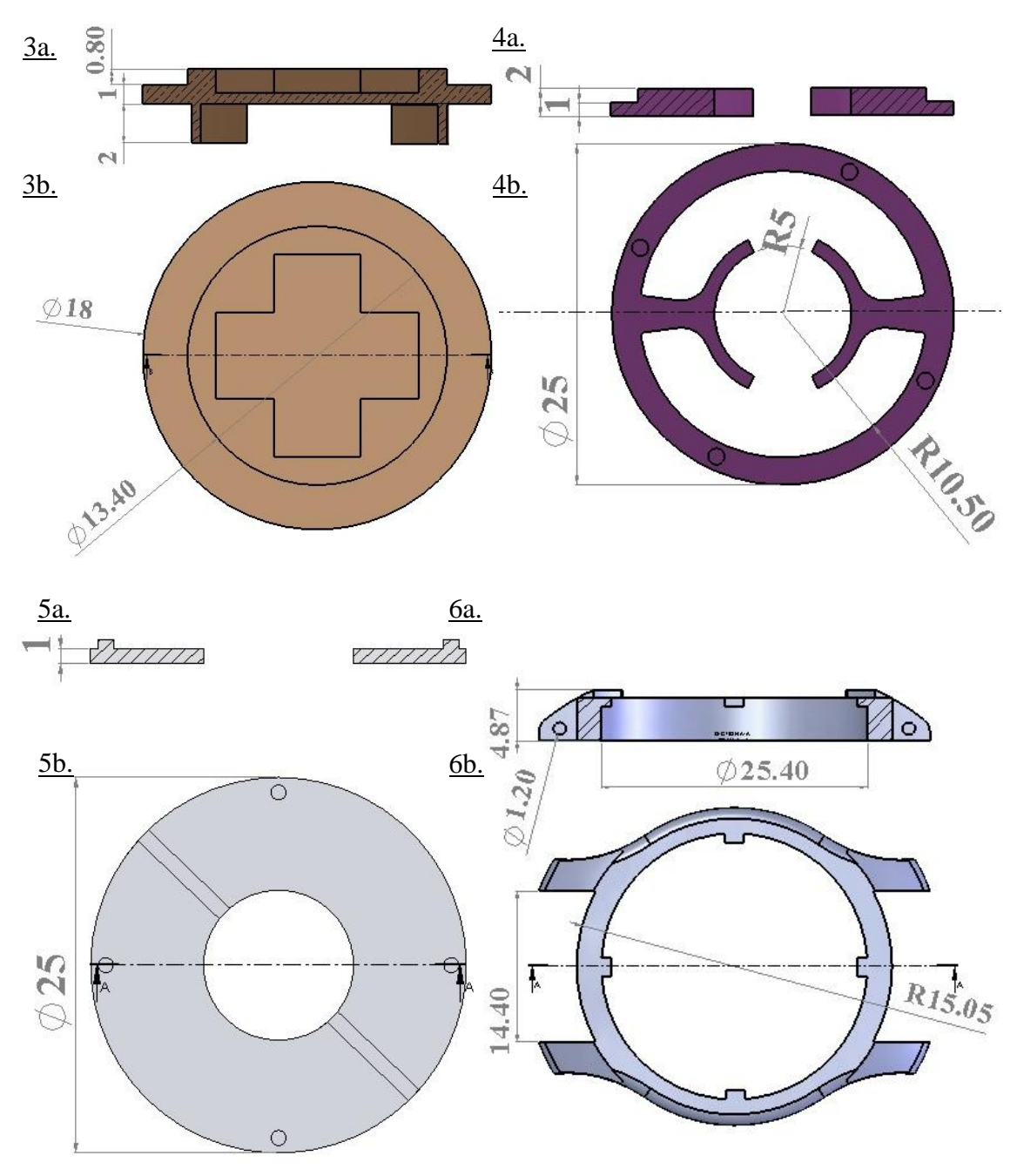


**Figure 2.7.** Second generation - structures of (1) key; (2) backing cover; (3) turnable cover; (4) swelling agent and hydrogel reservoirs; (5) insulin reservoir and (6) watch-like patch holder showing their dimensions and alignment feature. (a) Cross-sectional views across the dotted lines shown below and (b) surface views of the structures.

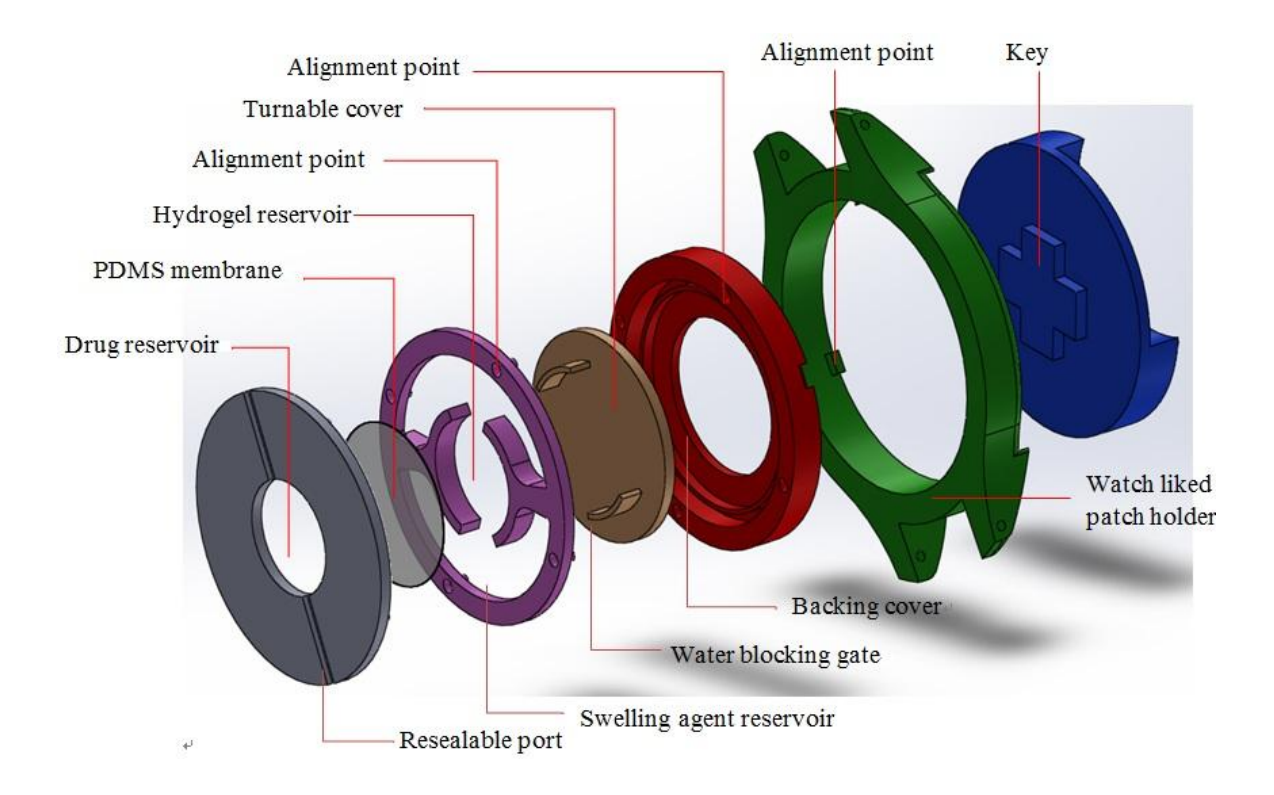


**Figure 2.8.** Expanded view of the second generation transdermal drug delivery patch.



**Figure 2.9.** A prototype of the second generation assembled patch.

#### 2.2.6. Assembly of the transdermal patch

All rapid prototyping products were coated with conformal silicone before assembly to prevent water loss from the patch. The resealable ports for the water and drug reservoirs were formed with a mixture of silicone and curing agent (50:1 w/w), treated at 60 °C for 4 h. A double-coated adhesive tape, cut into circular shape of 16 mm in diameter, was placed above the drug reservoir with the side facing the hydrogel reservoir. The area of the tape exposing to the drug reservoir was trimmed out, to which the PDMS membrane was then attached. Next, a prepared hydrogel was fitted into the hydrogel reservoir. The drug reservoir was assembled with the hydrogel reservoir by means of the alignment structures and bonded with superglue, followed by epoxy adhesive to ensure proper sealing and leakage-free. A microneedle plate, that was trimmed to appropriate size if necessary, was bonded to the drug reservoir (opposite side to the PDMS membrane) by silicone adhesive.

## 2.2.7. Hydrogel swelling characterization

In order to observe hydrogel swelling phenomena, two transparent polymethyl methacrylate (PMMA) substrates for the drug, water, and hydrogel reservoirs were fabricated (see Figure 2.10). The hydrogel swelling characterization setup is shown in Figure 2.11. The substrate for the water and hydrogel reservoirs was placed at the bottom while that for the drug reservoir was at the top. A PDMS membrane was placed between the two substrates. A dried hydrogel was put inside the hydrogel reservoir. Weight was applied on top to hold the assembled substrates in place. DI water was added to the water reservoir to initiate hydrogel swelling. Photos were taken hourly for 8 h after water addition.

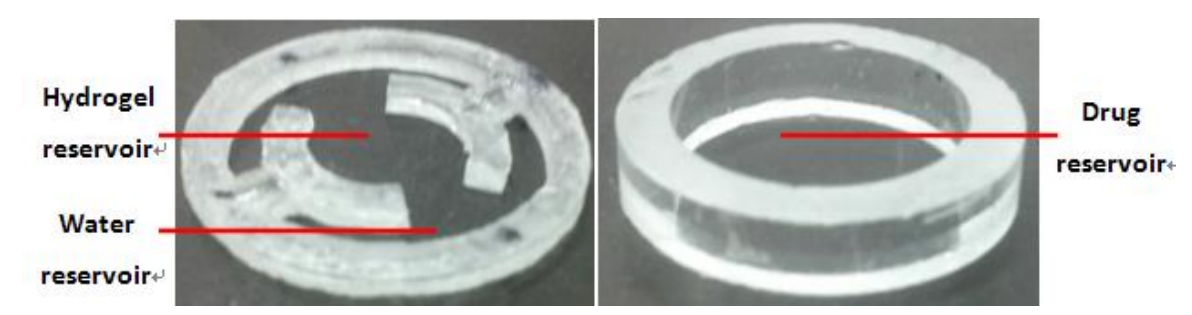


**Figure 2.10.** Transparent substrate for hydrogel swelling characterization.



Figure 2.11. Setup for hydrogel swelling characterization.

### 2.2.8. Preparation of porcine ear back skin

Porcine ears were freshly obtained from local slaughter, gently washed with running tap water, and chopped into pieces of 50 mm in width. Visual observation was done to check if the skins were free from lesions and infections. Hairs at the back of the ear were carefully removed by clipper. Full-thickness skins were obtained using manual-operated dermatome with uniform insertion force and angle. The skins were cut into discs of 40 mm in diameter. The skins were then sprayed and rubbed with 75%

ethanol for 1 min to remove fatty tissues and dirt, followed by DI water washing [77]. Thereafter, the skins were blotted with kimwipes, wrapped with aluminium foil, and stored in a -20 °C refrigerator until further use. All prepared porcine skins were used within 2 weeks.

#### 2.2.9. Skin insertion test

Porcine skin was thawed at room temperature for 1 h before the start of experiment. Diluted EB (50  $\mu$ L) and DI water (400  $\mu$ L) were loaded into the drug and water reservoirs, respectively. Adhesive tapes were attached to the patch and skin for even force distribution. After 6 h, images were captured by placing the samples under (side of the stratum corneum facing) as well as above (side of the dermis facing) a lighting system.

# 2.2.10. Drug permeation test in vitro

Vertical diffusion cell was filled with 7 mL phosphate-buffered saline (PBS) (137 mM NaCl, 2.7 mM KCl, 4.3 mM NaH<sub>2</sub>PO<sub>4</sub>  $7H_2$ O, and 1.6 mM KH<sub>2</sub>PO<sub>4</sub>, pH 7.4) and

pre-run at 300 rpm with bath circulator for 1 h to achieve 37 °C [78]. Processed porcine skin was thawed by soaking into PBS solution at room temperature for 1 h. After that, the porcine skin was blot-dried and mounted between the receptor and donor cells of the diffusion system. The stratum corneum of the skin faced the donor cell while the dermis side faced the receptor cell. The skin was handled with care to avoid bubble accumulation on the receptor side of the skin. Model drugs (70 µL) and DI water (400 μL) were loaded into the drug and water reservoirs of the patch, respectively, through the resealable ports. The patch was gently shaken to ensure water can make contact with the dried hydrogel inside. The patch was applied on the donor side of the skin by finger force, with the help of adhesive tapes to keep the patch in position. Samples (1 mL) were withdrawn from the receptor cell every hour with immediate replenishment of the same volume of fresh PBS. The tests were done with patches bonded with ME-C-600, SSM-O-150, or P-O-500. Three model drugs including MB (90 µM), DFS (10 mg/mL), and FITC-insulin (1 mg/mL) were tested accordingly. Active infusion (AI) was achieved by triggering hydrogel swelling with swelling agent injection. Diffusion (DF) was achieved without swelling agent addition to prevent hydrogel swelling. Positive Control

was achieved by injecting same amount of drug models into receptor chamber of the diffusion using 21 gauge number needle. Negative control was achieved by placing a plain (without any microneedle) plate-adhered patch on porcine skin with hydrogel swelling triggered. Quantification of MB was done by UV–vis spectrophotometer with absorbance at 664 nm. Determination of DFS concentration was accomplished by UPLC with gradient method A:B from 70%:30% to 10%:90% to in 4 min where A is 0.02% trifluoroacetic acid (TFA) in  $H_2O$  and B is 0.02% TFA in acetonitrile (ACN) (detection wavelength = 210 nm, flow rate = 0.45 mL/min). FITC-insulin release was quantified by measuring the fluorescence with excitation and emission wavelengths of 492 nm and 520 nm, respectively. Samples were quantified with reference to standard curves obtained from known concentrations of the model drugs.

# **2.2.11.** In vivo test

Diabetes was induced in rats using single injection of 65 mg/kg streptozotocin [79] (Animal license reference number: (10-558) in DH/HA&P/8/2/1 Pt. 16). Rats were harvested for 3 hours before the start of tests. The hairs from the back of the DM rats

were removed using chemical depilatory cream containing thioglycolate. The rats were anesthetized by a ketamine/xylazine solution. After that, the rat skin was exposed to an excess of PBS buffer as negative control. A rat was intradermally injected with 0.1 IU and 0.2 IU insulin to serve as positive controls. 70 µL of 2.85 IU/mL insulin was loaded into a second generation transdermal patch with P-O-500. Delivery was triggered by swelling agent loading as described in Section 2.2.5. The device was placed on the rats' back and held in position by wrapping the watch band around the rats' body as illustrated in Figure 2.12. Blood samples were withdrawn by tail incisions from the rats. The blood glucose level (BGL) of rats was recorded hourly using a portable glucose meter.



**Figure 2.12.** Insulin-loaded second generation transdermal patch attached to a diabetes mellitus (DM)-induced rat.

# **Chapter 3**

#### **Results and Discussion**

# 3.1. Visualization of hydrogel swelling

This test aims to verify that the expansion force from hydrogel swelling is sufficient to deflect the PDMS elastic membrane below to the drug reservoir and force the drug out from the microneedles. It is also important to observe the hydrogel swelling rate to check if the volume expansion as well as drug release rate meet our proposed needs. From Figure 3.1, the hydrogel started swelling after water addition, reached about half of the height of the PMMA tube (approximately 1.2 mm) in 2 h, and then swelled very slowly afterward. The result clearly indicates that the swelling force from the hydrogel is sufficient to deflect and force the PDMS membrane toward the drug reservoir. Nevertheless, the swelling process is too fast for long-term delivery (e.g., 8 h).

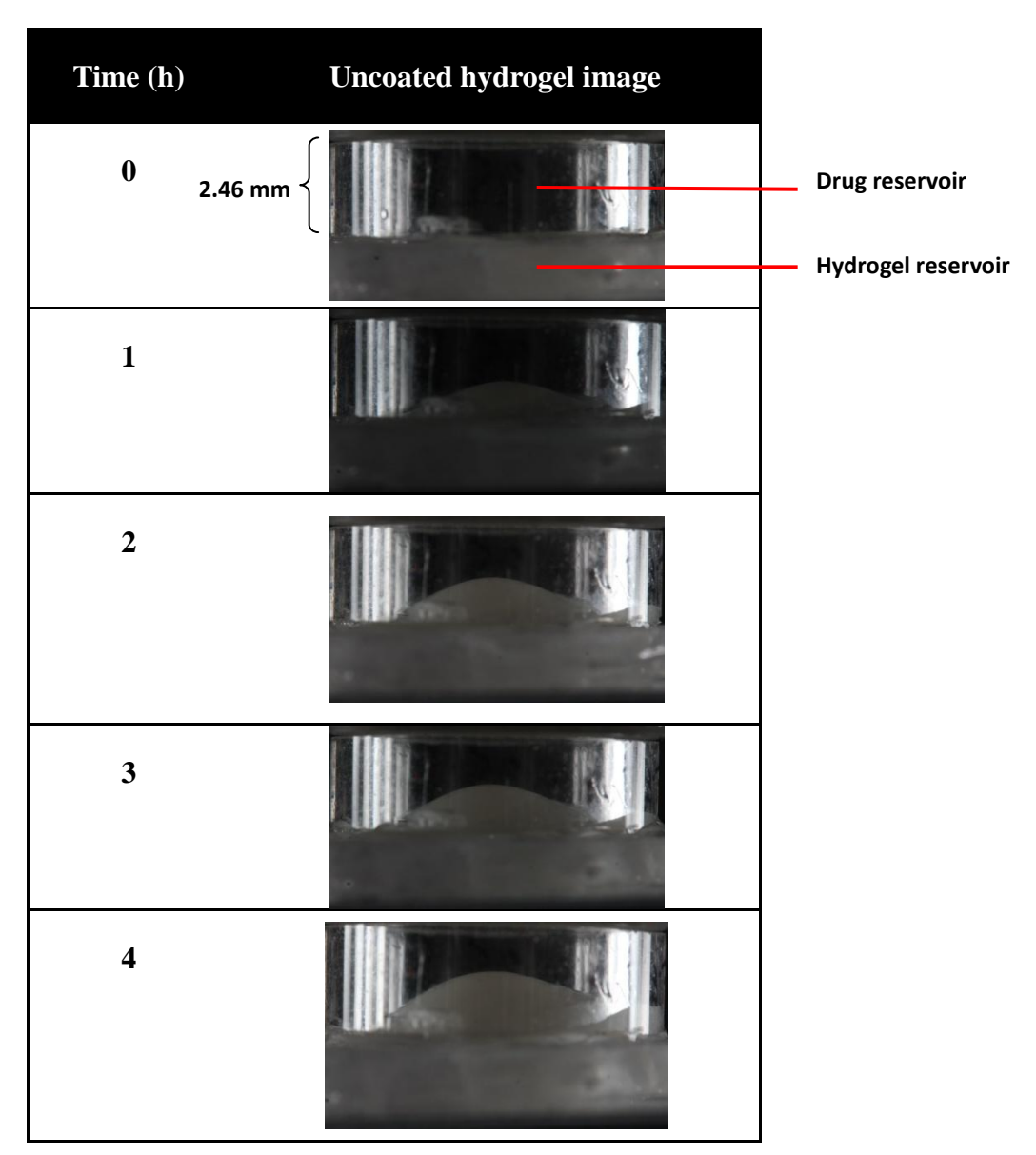


**Figure 3.1.** Swelling property of uncoated hydrogel over time.

To achieve a slower yet controlled hydrogel swelling, a PDMS coating was employed to hinder water contact of the dried hydrogel. A spray coating step was carried

out, as detailed in Section 2.2.3. To verify the coating of PDMS onto the hydrogel, a spray-coated sample was examined under scanning electron microscope (SEM). The SEM samples were prepared by cutting out half of a laminated layer from the hydrogel surface, followed by careful peeling using forceps. A coated surface can be easily distinguished from the uncoated one as the PDMS layer is reflective under light while the hydrogel rough surface is dull and non-transparent. Figure 3.2 shows that PDMS of a thickness of 51.7 µm was coated onto the hydrogel.

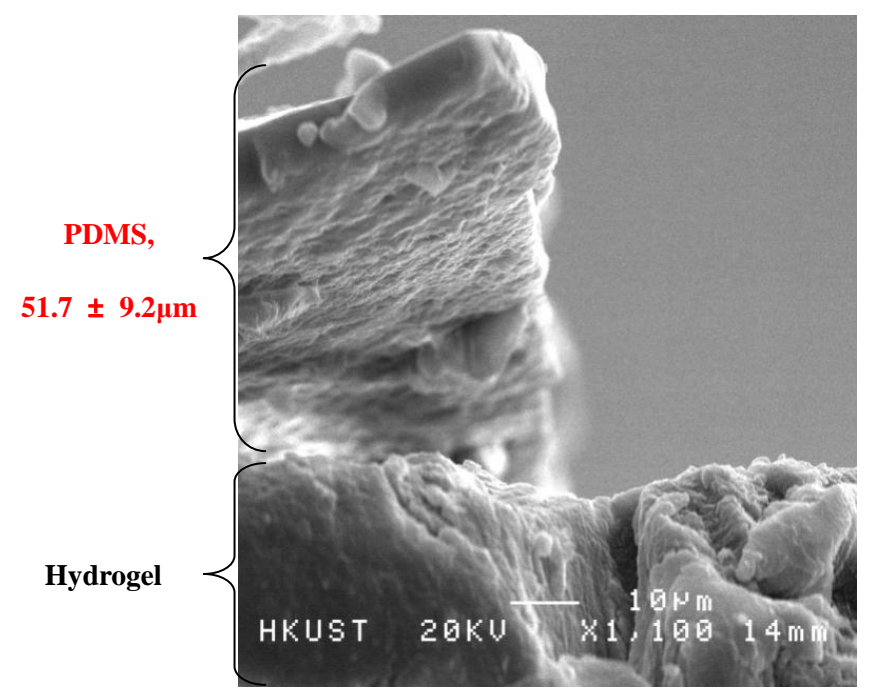


**Figure 3.2.** Cross-sectional view of a polydimethylsiloxane (PDMS)-coated hydrogel under scanning electron microscope (SEM).

The swelling property of the coated hydrogel was then compared with the uncoated one (Figure 3.3). Despite the difficulty in quantifying the volume expansion of the hydrogel by camera, the prolonged swelling process after coating was clearly observed.

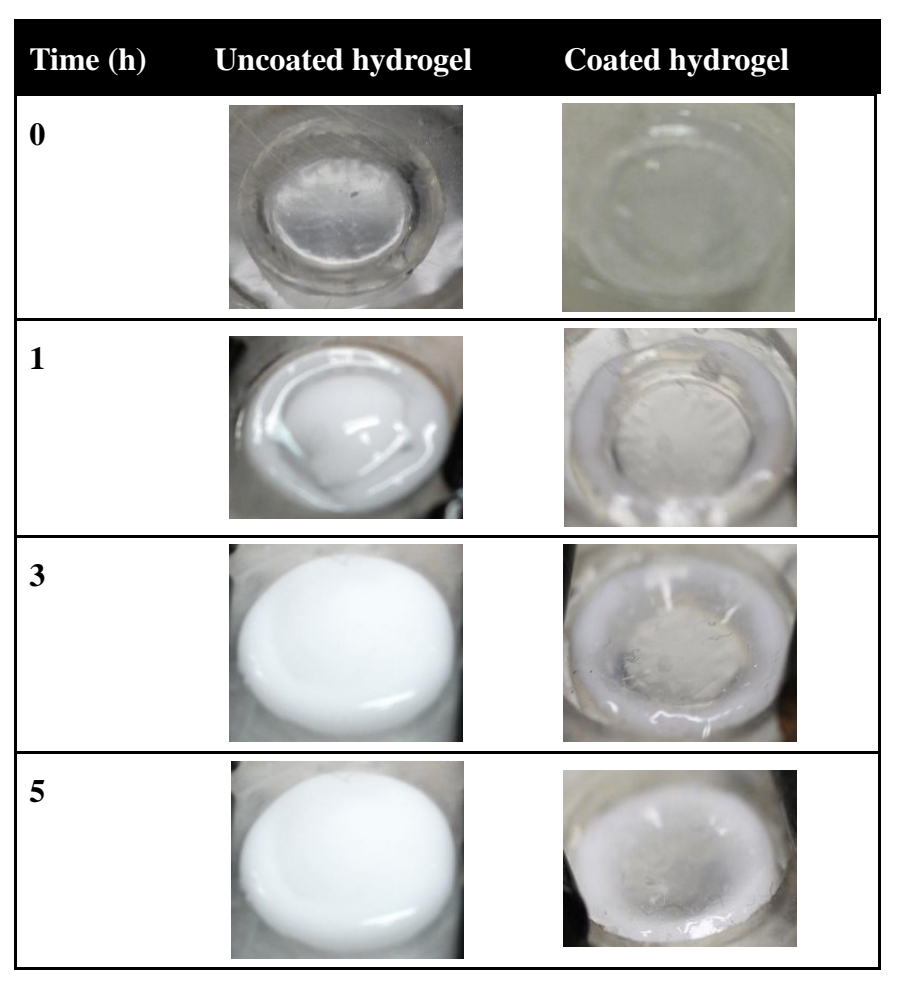


Figure 3.3. Swelling properties of uncoated and coated hydrogel over time.

#### 3.2. Skin insertion tests by microneedles

Insertion tests were done to validate the ability of transdermal delivery by the microneedles. The microneedles were visually examined beforehand to ensure they were intact, as shown in Figure 3.4. EB was used for visualization in the insertion tests. A negative control (no microneedles) and three microneedle samples (ME-C-600, SSM-O-150, and P-O-500) were tested. The properties of microneedles are enlisted below:

**Table 2.** Properties of different types of microneedles.

	Types of microneedles		
	SSM-O-150	ME-C-600	<u>P-O-500</u>
Microneedle length (μm)	150	600	500
Material	Zeolite	Stainless Steel	Polyoxymethylene
Density (cm <sup>-2</sup> )	238	169	64

In the control group, no observable staining pattern was found on the sample when it is put under (side of the stratum corneum facing) and above (side of the dermis facing) a

lighting system (Figure 3.5), proving that the staining pattern afterward is not caused by follicles after hair removal.



**Figure 3.4.** [Left] stainless steel microneedle (ME-C-600) and [middle] plastic microneedle (P-O-500) under camera, as well as [right] stainless steel microneedle (SSM-O-150) under scanning electron microscope (SEM).

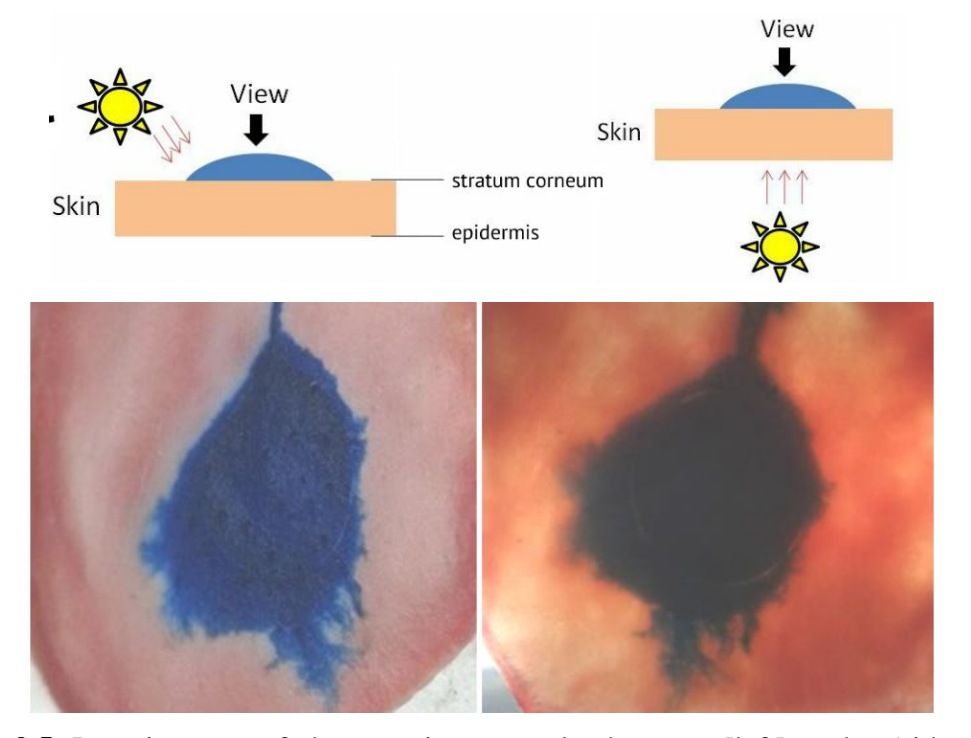


**Figure 3.5.** Insertion test of the negative control when put [left] under (side of the stratum corneum facing) as well as [right] above (side of the dermis facing) a lighting system.

The porcine skin mounted with the commercial microneedle (ME-C-600) did not show observable fissures under light (Figure 3.6, left image). But small holes that were not dyed with EB were visualized when the skin was put above light (Figure 3.6, right image). The pattern of holes is different from that of the hair follicle in the porcine skin. It is because ME-C-600 is solid-type microneedles that pierce the skin and prevent EB from passing along the microneedles to the deeper layer of the skin, thereby leading to the unstained holes.

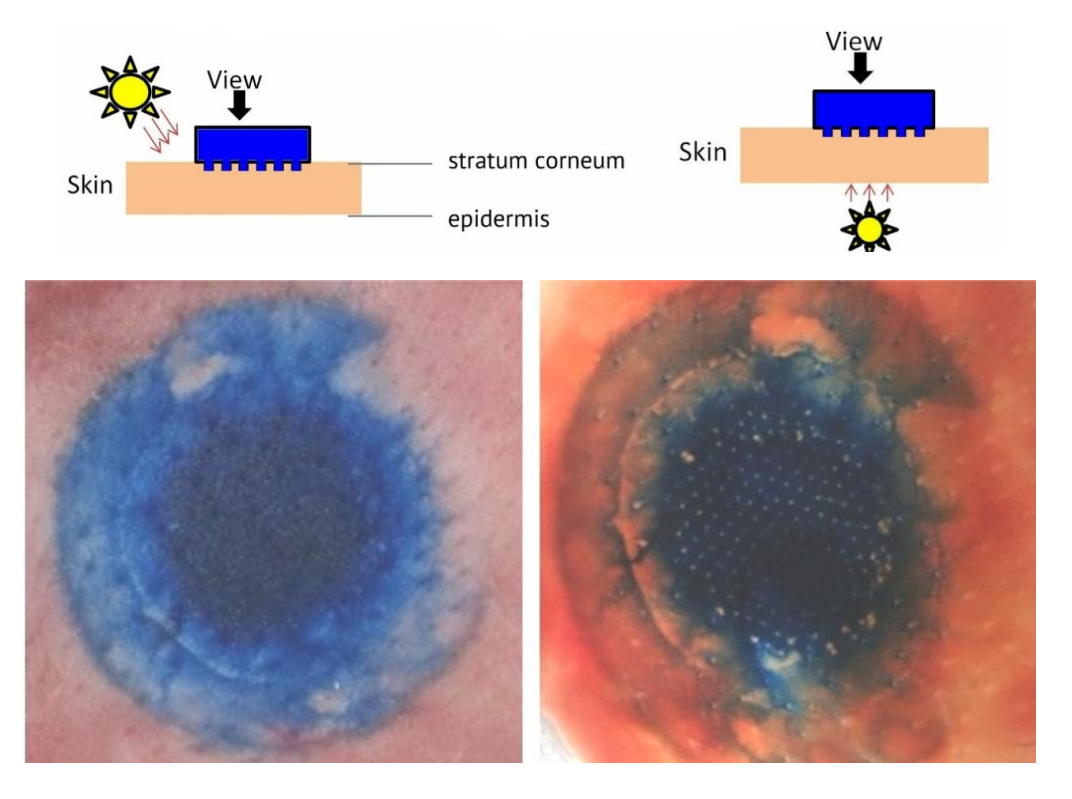


**Figure 3.6.** Insertion test of stainless steel microneedle (ME-C-600) when put [left] under (side of the stratum corneum facing) as well as [right] above (side of the dermis facing) a lighting system.

For zeolite microneedles (SSM-O-150), yellowish regions were observed under light, which were caused by the rust of the SSM plate during microneedle growth (Figure 3.7, left image). Yet, dyed holes were observed on the skin (circled regions). These holes existed in different patterns and sizes than the hair follicle. They are believed to be caused by the SSM-O-150 microneedles. Since the SSM-O-150 microneedles are hollow, EB can pass through the channels of the microneedles and to the deeper layer of the skin, forming deep blue-colored holes when compared to EB on the top skin layer.

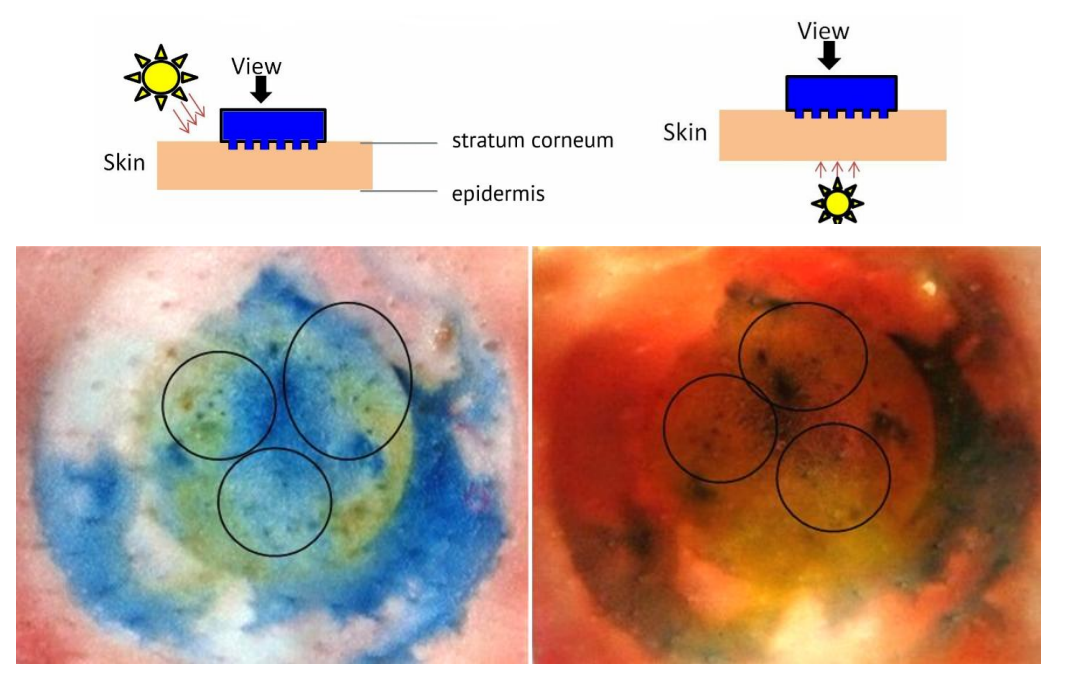


**Figure 3.7.** Insertion test of zeolite microneedle (SSM-O-150) when put [left] under (side of the stratum corneum facing) as well as [right] above (side of the dermis facing) a lighting system.

For P-O-500 microneedles (4  $\times$  4), only the central 4 microneedles were used for EB delivery as the peripheral space was reserved for patch adhesion. Hence, in Figure 3.8 (right image), it can be seen that the peripheral 12 microneedles remained unstained while the central 4 microneedles delivered EB into the deeper skin layer to form stained points.

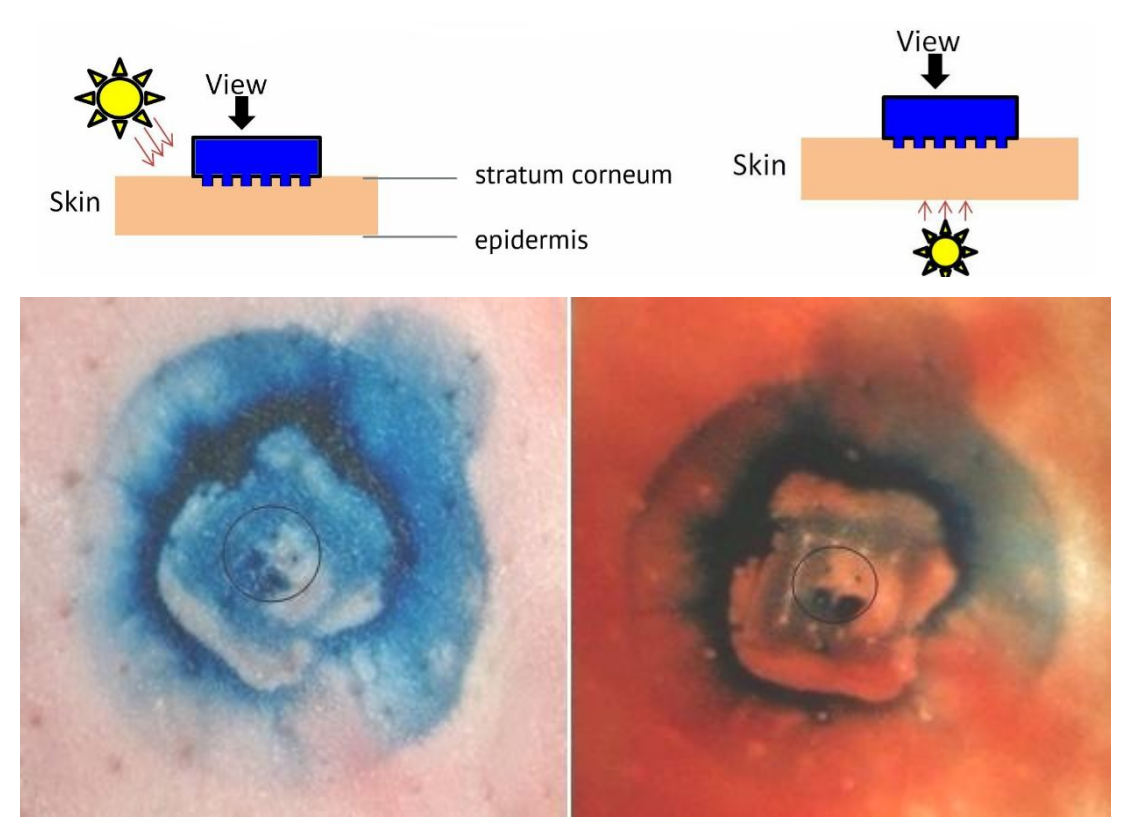


**Figure 3.8.** Insertion test of plastic microneedle (P-O-500) when put [left] under (side of the stratum corneum facing) as well as [right] above (side of the dermis facing) a lighting system.

## 3.3. In vitro drug permeation tests

#### 3.3.1. In vitro test – methylene blue

Porcine ear skin was used as the delivery barrier in the in vitro experiment because of the similar histological and physiological properties to human skin [80, 81]. MB was used as the model drug in the preliminary evaluation of drug delivery because its peak/optimum absorption wavelength is far away from that of interferences that exist in the porcine skin (e.g., protein), which influence the absorbance reading. It is also feasible to validate MB permeation through the skin by observing color change in the receptor chamber. Drug delivery by active infusion (AI) or diffusion (DF) can be controlled by adding or omitting DI water for hydrogel swelling, respectively. As shown in Figure 3.9, the absorbance of MB at 664 nm was plotted against different concentrations of MB to form a standard curve with R<sup>2</sup> value of 0.997.

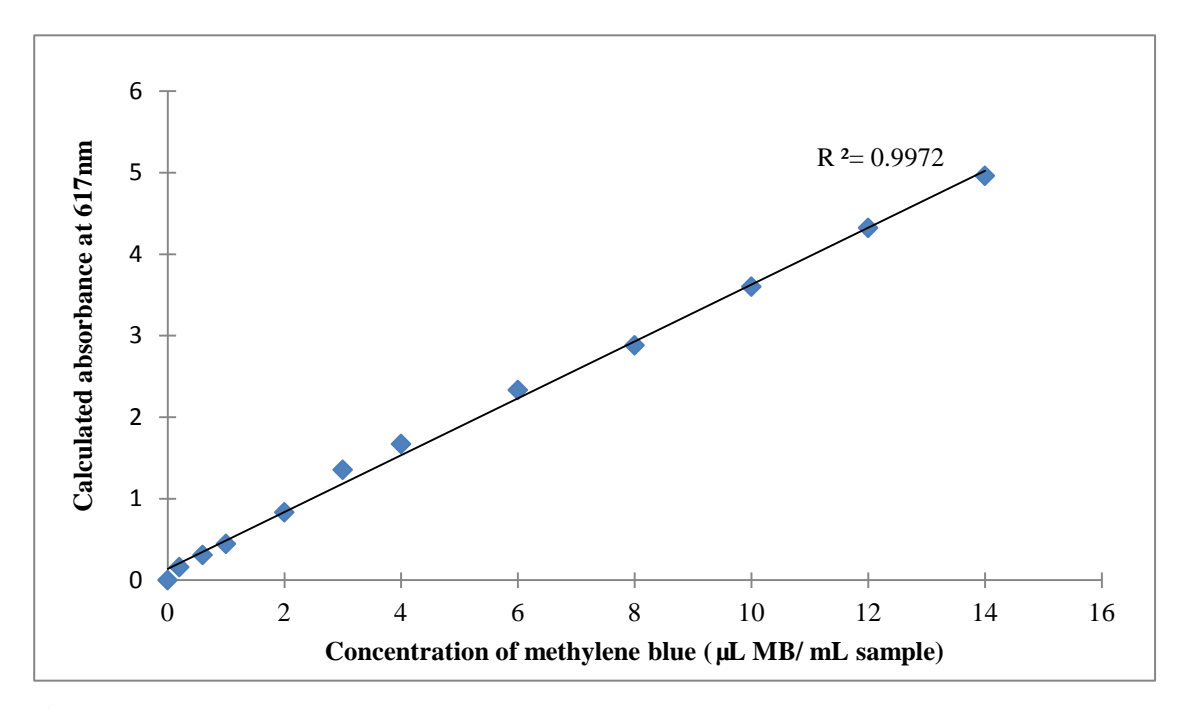


**Figure 3.9.** Standard curve for methylene blue (MB).

Figure 3.10 demonstrates the cumulative MB release by different delivery schemes. Diffusion of MB through the skin without microneedles (DF) exhibited limited delivery as the stratum corneum blocks most of MB from entering the skin. Active infusion without microneedles (AI) allows hydrogel swelling to force more MB out from drug reservoir in patch, releasing more MB for diffusion.

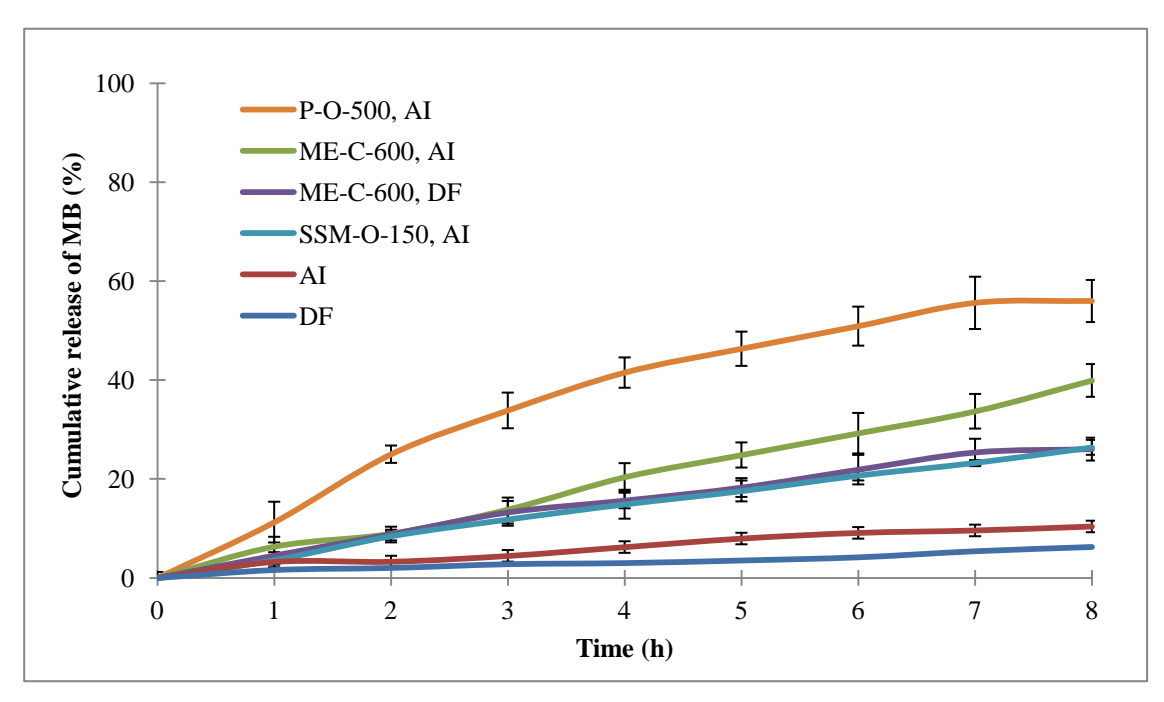
Patch performance was enhanced when the patch was coupled with microneedles (for all the three types of microneedles). Delivery of MB by the ME-C-600-adhered patch is at least double of that without microneedles. It is postulated that ME-C-600 (a

plate grown with solid microneedles) pierced into the skin to generate fissures. Solutes can diffuse through the fissures into the receptor chamber, thereby leading to the increased diffusion rate. The delivery rate further increased by means of active infusion.

With SSM-O-150 (a stainless steel plate grown with hollow zeolite microneedles), the efficiency is only about half of that of the ME-C-600 patch. One possible reason for the lower delivery rate of SSM-O-150 is shorter microneedle length (microneedle length of SSM-O-150 is 150 μm while that of ME-C-600 is 600 μm). In in vivo situation, drugs delivered exert their pharmaceutical effects only if they pass through the epidermis to reach the microcirculation system in the dermis (as discussed in Section 1.2). Longer microneedles shorten the solute diffusion distance from needle lumen to the circulation paths, resulting in a faster drug delivery to the receptor. Shorter diffusion path can also reduce the area of adsorption by peripheral protein matrix, and thus a higher amount of drug is delivered in the receptor. Another possible reason that affects drug permeability is the mechanical strength of the microneedles. Microneedles on SSM-O-150 are made of zeolite. Zeolite microneedles are relatively fragile compared to stainless steel microneedles on ME-C-600. Consequently, some of the zeolite microneedles may break

during skin piercing and fewer microneedles are available for drug delivery. This assumption can be supported by the uneven stained pattern in Figure 3.7 during the insertion test, indicating not all microchannels can deliver drug into the deeper skin layer.

P-O-500, in contrast, is a plate micromolded with 500-μm long plastic hollow microneedles. It possesses both unique characteristics of ME-C-600 and SSM-O-150 (long and hollow) to facilitate drug delivery. Its proven toughness can withstand repeated skin penetration without severe deformation or breakage. The delivery rate by P-O-500 is the best amongst the three microneedle samples. The R<sup>2</sup> from the first 5-h data of the test with a linear fit is over 0.98, and it decreases slightly to 0.96 over the entire 8-h period. The drug release for the first 5 h is zero-order, and the slight decline afterward may be the consequence of MB adsorption on the porcine skin, lack of DI water for hydrogel swelling, and/or hydrogel erosion.



**Figure 3.10.** In vitro tests using different types of microneedles: stainless steel microneedle (ME-C-600), zeolite microneedle (SSM-O-150), or plastic microneedle (P-O-500); and delivery mechanisms: diffusion (DF) or active infusion (AI).

#### 3.3.2. In vitro test – diclofenac sodium

The validation of diverse drug delivery by the patch was tested by choosing alternative drug. DFS, a common analgesic, was chosen as a model drug. All the data presented were collected from the patch with 2-layer sprayed-coated hydrogel. Quantification of DFS was by UPLC, a typical chromatogram is shown in Figure 3.11. A standard curve with  $R^2$  value > 0.999 is shown in Figure 3.12.

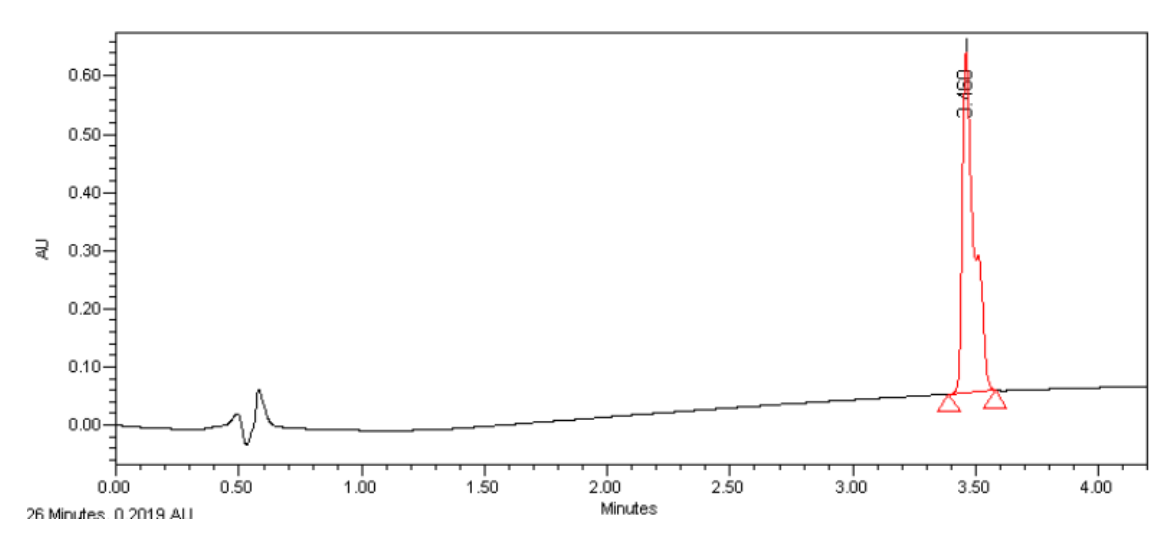


**Figure 3.11.** A chromatogram of 100 μg/mL diclofenac sodium (DFS) sample.

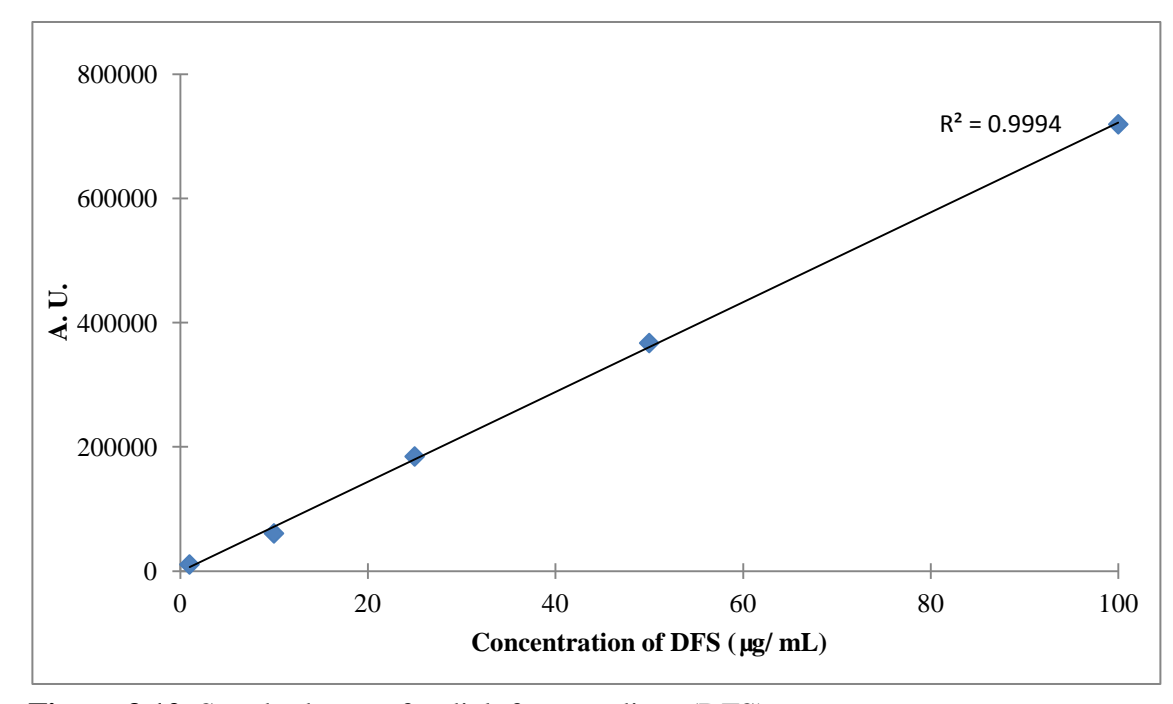
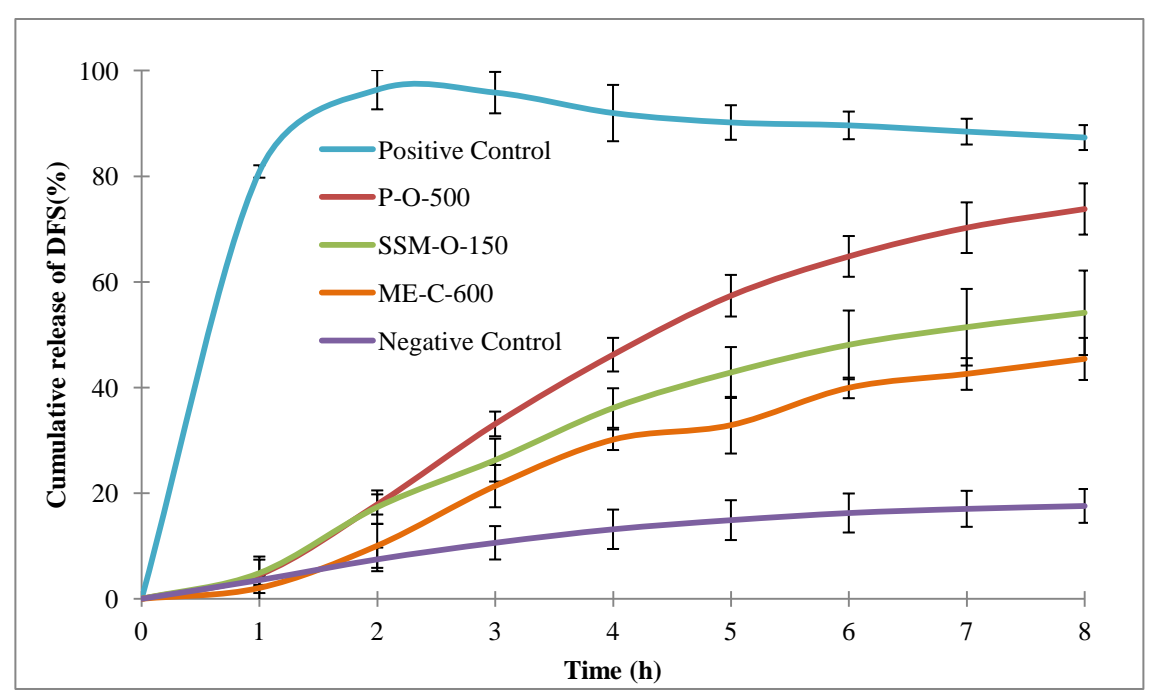


Figure 3.12. Standard curve for diclofenac sodium (DFS).

Figure 3.13 presents a graph of DFS delivery by active infusion transdermal microneedle patch with different types of microneedle plates. DFS exerts low bioavailability in transdermal application because of the stratum corneum in the outermost skin. Negative control was achieved by pipetting known amount of DFS onto the skin for diffusion. As expected, the amount of DFS transferred is relatively low. Percentage of DFS delivered (17.6  $\pm$  3.2%) after 8-hour testing is comparable with the result by Varghese's group (In a 6-hour test, the cumulative delivery of DFS by diffusion was between 11.1% and 17.9%, depending on the concentration) [82]. Plastic microneedle-adhered patch yields the highest DFS delivery with about 73.8  $\pm$  4.9% of drug delivered in 8-hour test. The delivery is linear with R<sup>2</sup> value = 0.9704.



**Figure 3.13.** Cumulative release of diclofenac sodium (DFS) by patches with different types of microneedles.

# 3.3.3. In vitro test – FITC-insulin

It is particularly important to evaluate insulin delivery based on the research objectives. The negative control (direct pipetting known amount of insulin onto the stratum corneum of the skin) showed little permeation across the barrier (3.7  $\pm$  1.1%) as insulin is too large (~55 kDa) for direct skin penetration. In contrast, 78.7  $\pm$  4.3% of FITC-insulin was delivered by P-O-500-adhered patch. The insulin delivery was

reduced to 51.5  $\pm$ 7.5% with SSM-O-150-bonded patch. This may be due to insulin loss to the peripheral skin through the broken zeolite microneedle array.

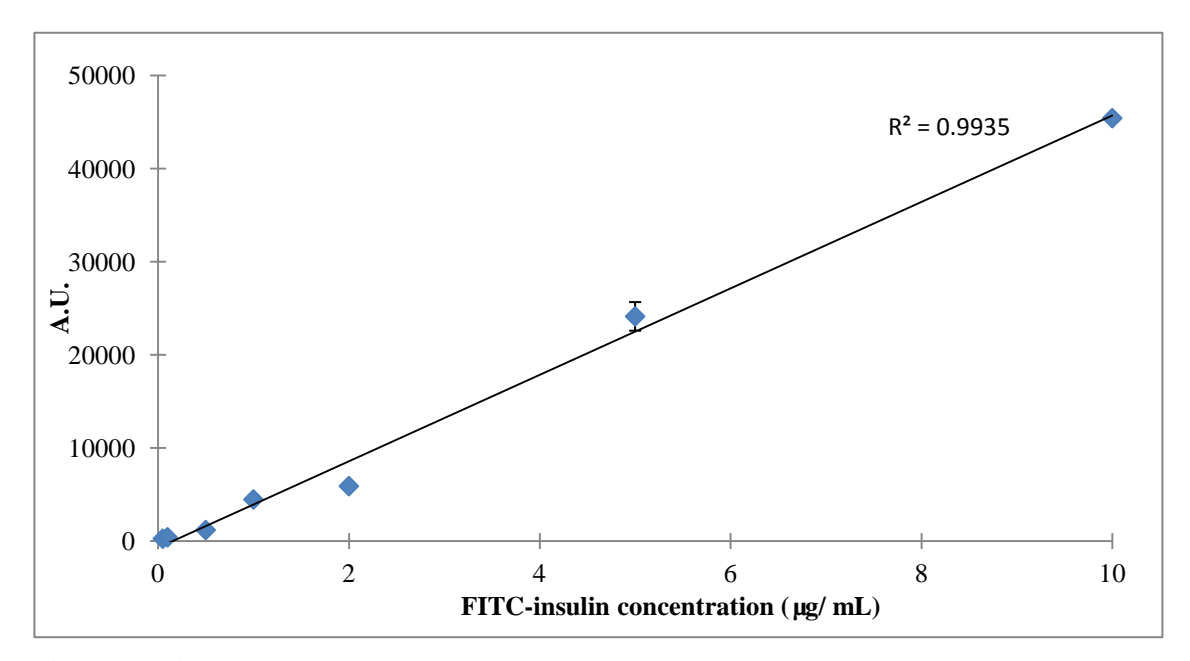
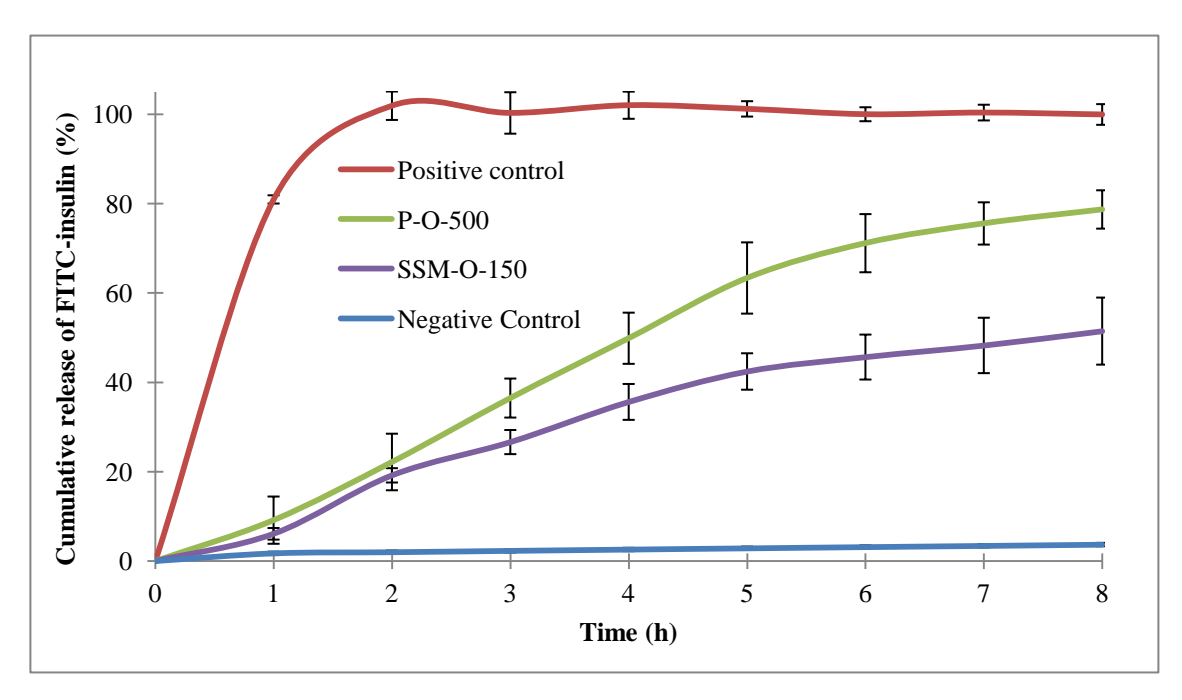


Figure 3.14. Standard curve for fluorescein-tagged insulin (FITC-insulin).



**Figure 3.15.** Cumulative release of fluorescein-tagged insulin (FITC-insulin) by patches with different types of microneedles.

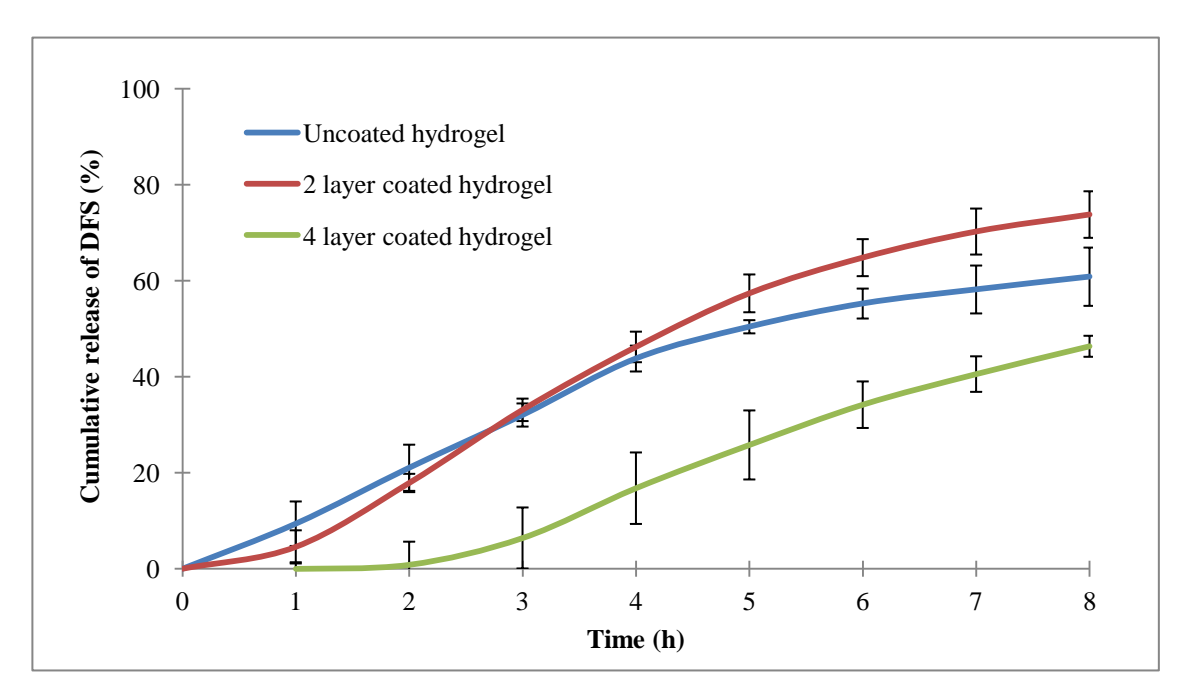
# 3.3.4. Effect of coating hydrogel with PDMS on drug delivery efficiency

Figure 3.16 illustrates the effect of number of spray-coating layers (coating of hydrogel with PDMS) on in vitro drug (DFS) delivery efficiency. P-O-500 was used in the experiment. The delivery by P-O-500-adhered patch with uncoated hydrogel increases exponentially at the initial stage, and starts to level off after 4 hours of testing. In contrast, DFS delivery with 2-layer-coated hydrogel is slower initially but becomes

faster at the later stage. After 8-hour testing, the amount of drug delivered by the patch with 2-layer-coated hydrogel is surprisingly higher than that of the uncoated hydrogel. This can be explained by the gel swelling kinetics. For the uncoated hydrogel, the swelling agent can immediately make contact with the dried hydrogel, leading to a rapid and localized swelling at the gel surface. According to the explanation by Singh et al., the gel boundary moves inward in a rapid manner [83]. The peripheral swelling of the hydrogel hampers the diffusion of swelling agent from the outside to the center of the hydrogel, leading to incomplete hydrogel swelling even at the end of the test. On the other hand, the PDMS layer coated on the hydrogel can block excessive swelling agent diffusion to the hydrogel at the beginning. The limited movement of gel boundary allows more sufficient diffusion of the swelling agent to the center of the hydrogel, resulting in relatively complete swelling of the whole hydrogel at the end.

For the 4-layer-coated hydrogel, such thick coating allows more complete hydrogel isolation from the swelling agent as well as larger opposing force against the hydrogel's swelling. As a result, volume expansion of the hydrogel is hindered at the first 3 hours of the test and hence less amount of drug is forced out. The hindrance by the coating is,

however, outweighed by the strong polymer dispersion force in the later stage. Similar to the 2-layer-coated hydrogel, the presence of water-resistant coating provides a crucial factor for zero-order hydrogel swelling. It is also worth noticing that, at the start of the test, the swelling of the 4-layer-coated hydrogel varies greatly among different trials, and such variation is reduced at longer times. It means that the time of PDMS layer breakage varies between tests but eventually the extents of hydrogel swelling are similar. The amount of drug delivered with the 4-layer-coated hydrogel (50.8  $\pm$  2.2%) is smaller than that with the uncoated hydrogel (60.9  $\pm$  6.1%) and the 2-layer-coated hydrogel (73.8  $\pm$  4.9%). It indicates that the 4-layer-coated hydrogel is not fully swollen after 8 hours of water contact. Nevertheless, this may enable controlled drug release in a longer time frame (e.g., 12 h or longer).



**Figure 3.16.** Cumulative release of diclofenac sodium (DFS) by plastic microneedle (P-O-500)-adhered patch with hydrogel having different layers of polydimethylsiloxane (PDMS) coating.

## 3.3.5. Delivery of different drugs by P-O-500-bonded patch

The in vitro cumulative release of DFS (70.2  $\pm$  4.8%) and FITC-insulin (75.6  $\pm$  4.7%) are comparable in 8-hour testing, while that of MB is lower (55.6  $\pm$  5.3%). MB delivery starts to level off in the later stage of the experiment. The lower release of MB is believed to be caused by the ease of dye adsorption by the porcine skin. MB is a medical dye for cell staining. It practically does not stain epidermal keratin because of

the stabilized structure of the insoluble keratin bundles during cornification. On the contrary, MB accumulates in the dermal tissue due to the interaction with protein molecules in the interstitial fluid. The similar delivery patterns of DFS and FITC-insulin indicates that the use of microneedle may provide similar drug delivery rate regardless of the characteristics of the drugs (i.e., size, charges, and lipophilicity) as the microneedles provide microchannels that pass through the rate limiting barrier (i.e., the stratum corneum).

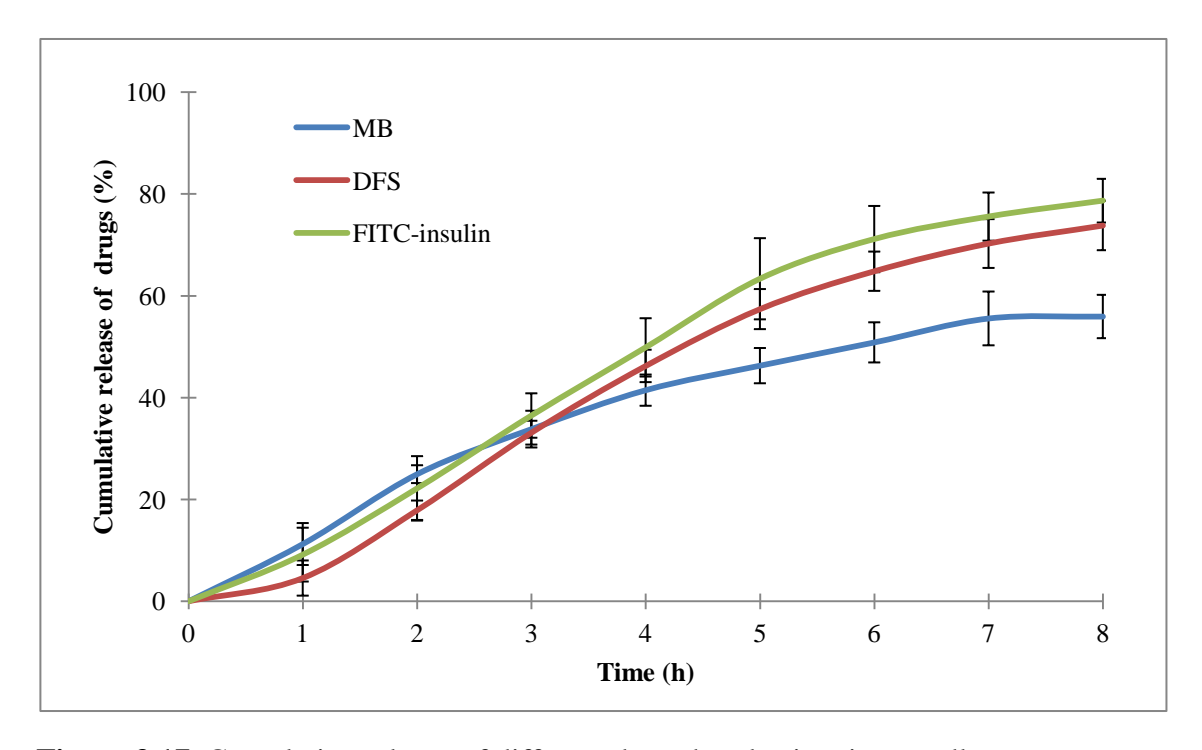


**Figure 3.17.** Cumulative release of different drugs by plastic microneedle (P-O-500)-adhered patch.

#### 3.4. In vivo test – insulin

In Figure 3.18, PBS solution injection serves as a negative control for the animal test (rat model). Progressive rise of BGL in the negative control is due to physiological change induced by stress hormones during fight-or-flight response under stressed environment (i.e., anxiety). Understandably, intradermal injection of higher concentration (0.2 IU) of insulin exerts higher pharmacological effect (lower BGL) than that of lower one (0.1 IU), and it takes longer time to resume to its normal BGL by haemostasis. Compared to syringe injection of the same concentration of insulin, BGL is slightly higher in the first two hours with plastic microneedles. Then, from 3 to 4 hours after administration, BGL with plastic microneedles becomes lower than that with syringe injection. After 6 hours, BGL with both delivery methods are almost the same. It could be explained by the continuous delivery of insulin from the patch that less insulin was delivered to the rats initially compared to bolus intradermal injection. Importantly, the continuous delivery prolongs the pharmacological effect, which permits basal insulin therapy.

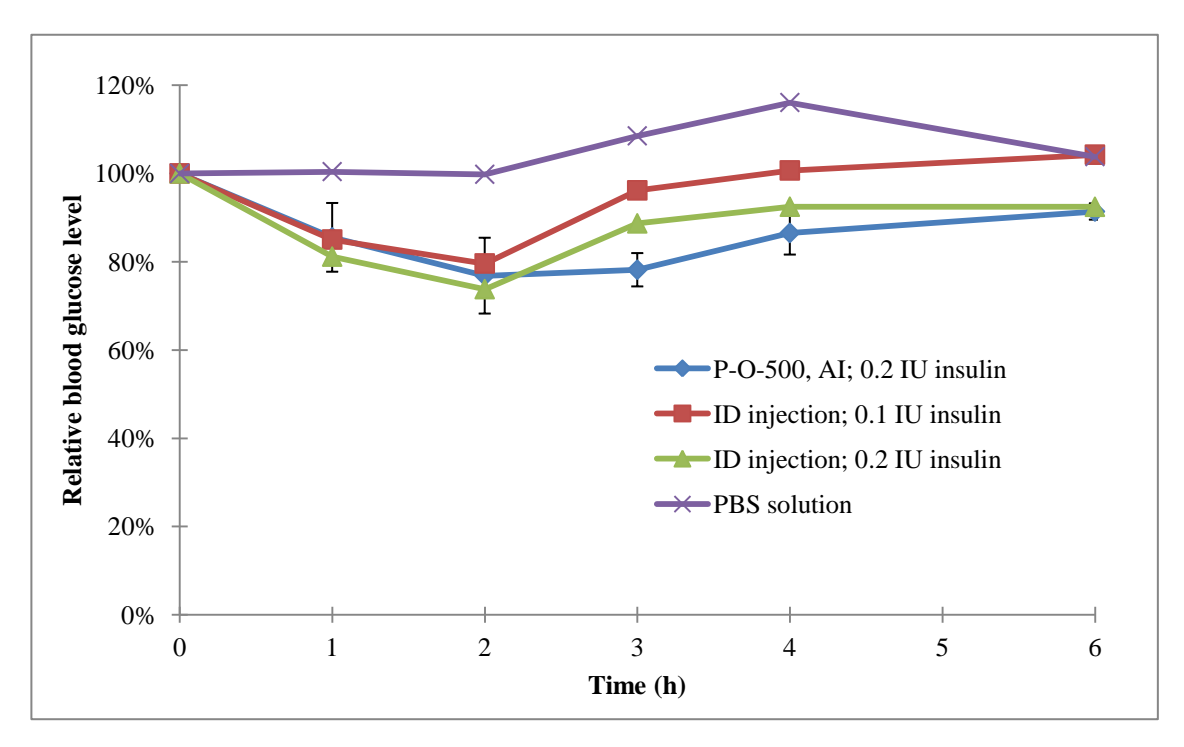


**Figure 3.18.** Blood glucose level change in response to insulin administration by various approaches.

# 3.5. Feasibility of scaling up production

Features of low cost and disposability from transdermal patch are highly desirable in terms of gaining broad acceptance and hygienic issues. Despite the rapid-prototyped patch in this research is costly for daily drug administration (material cost at around HK\$20 each), the cost can be greatly lowered if it is mass produced by injection molding. Figure 3.18 shows a rough estimation of the cost of fabricating 10<sup>5</sup> copies of the patch by injection molding (less than HK\$2 each). The cost can be further reduced if

the production quantity increases. The layer-by-layer structure of the patch makes it possible to be assembled by stepwise automatic laminations. Moreover, synthesis procedures of the hydrogel and PDMS membrane (i.e., curing, washing, and cutting) are easily to be scaled-up.

Ease of sterilization is yet another concern to provide disease-free delivery. Medical grade polyvinyl chloride and heat resistant acrylonitrile butadiene styrene are suitable raw materials because of their ability to withstand high temperature and pressure during autoclaving [84]. Other non-autoclavable materials can also be used with sterilization by gamma ray irradiation [85].

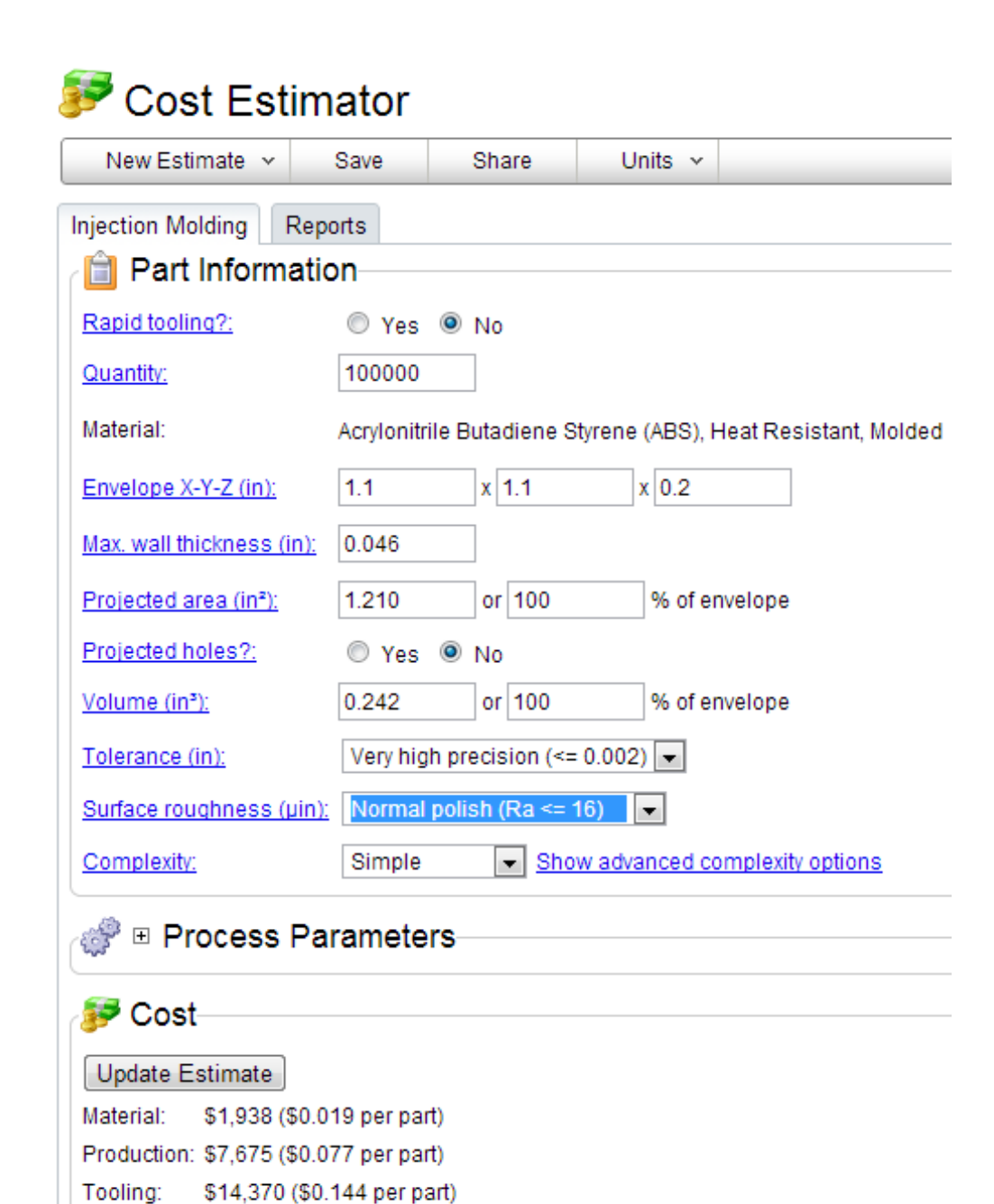


**Figure 3.19.** A cost estimation of patch made by injection molding (adopted from <a href="http://www.custompartnet.com/estimate/injection-molding/">http://www.custompartnet.com/estimate/injection-molding/</a> [86]).

\$23,983 (\$0.240 per part)

Total:

# **Chapter 4**

### **Conclusions and Recommendations for Future Work**

# 4.1. Key findings and conclusions

Development of a low-cost and disposable transdermal steady drug delivery patch with high compliance is highly desirable for patients especially in developing countries. This thesis aims to invent an active infusion-featured platform with the assistance of microneedles. In this study, hydrogel actuator had shown its capability of deflecting PDMS membrane towards drug reservoir. Spray-coated PDMS layer on hydrogel could successfully delay the hydrogel swelling. Drug permeation rate was improved by means of active infusion regardless of the choice of microneedles. Besides, patches adhered with P-O-500, ME-C-600 and SSM-O-150 also show relative linear drug delivery of which P-O-500-adhered patch releases more drug content from reservoir in 8 hour testing. In addition, P-O-500-bonded patch using 2-layer-coated hydrogel as actuator gave higher and more steady drug release than uncoated and 4-layer-coated hydrogel in 8-hour in vitro test. Moreover, the patch provided comparable drug release trend in two

commonly used drugs (DFS and insulin). Furthermore, the patch exerts its prolonged pharmacological benefit over bolus therapy in insulin delivery to DM-induced rats. To conclude, the simplicity of design and layer-by-layer framework allow mass production of the patch in order to achieve low-cost, disposable, and continuous drug delivery.

#### 4.2. Recommendations for future work

On the basis of the current delivery scheme, a series of investigations could be carried out. First of all, the drug delivery rate could be further enhanced. This can be accomplished by optimizing the hydrogel swelling rate such as type of polymer, concentrations of porogen, crosslinker, and initiation system [87, 88].

Second, the current patch dimensions can only hold up to 70  $\mu$ L drug that may not be suitable for large volume dose. To address this issue, the diameter of the patch as well as the hydrogel should be modified. It is also important to investigate the correlation between the height of reservoirs/hydrogel and the delivery rate.

Third, in addition to MB, DFS, and insulin, the drug models of this delivery device can be extended to other molecules such as DNA for gene therapy and immunogens

[89-92].

Last but not least, the swelling kinetics of PDMS spray coated hydrogel could be studied and correlated with parameters of the spraying process (i.e. spray coating time, pressure, number of coating and etc.). A mathematical model correlating material properties and the swelling ability could then be set up. This may be accomplished by data acquisition under nuclear magnetic resonance to capture the interaction between swelling agent and hydrogel framework.

#### References

- [1] S. Buavaroon, S. Supachai, B. Gordon, D. Sunthorn, B. Kittiphong, T. Alisa, and J. Sathaporn, "The therapeutic and clinical drug review of Thai traditional herbal remedies extracted from ancient Thai medicinal manuscript," *Advances in Natural Science*, vol. 5, pp. 29, 2012.
- [2] Y. C. Jang, "Infectious/medical/hospital waste: general characteristics," *Encyclopedia of Environmental Health*, pp. 227-231, 2011,
- [3] K. E. Thummel, K. L. Kunze, and D. D. Shen, "Enzyme-catalyzed processes of first-pass hepatic and intestinal drug extraction," *Advanced Drug Delivery Reviews*, vol. 27, pp. 99-127, 1997.
- [4] G. Chopda, "Transdermal drug delivery systems : a review," *Pharmaceutical Reviews*, vol. 4, 2006.
- [5] A. A. Barba, M. d'Amore, S. Cascone, S. Chirico, G. Lamberti, and G. Titomanlio, "On the behavior of HPMC/Theophylline matrices for controlled drug delivery," *Journal of Pharmaceutical Sciences*, vol. 98, pp. 4100-4110, 2009.
- [6] C. C. Apfel, K. Zhang, E. George, S. Shi, L. Jalota, C. Hornuss, K. E. Fero, F. Heidrich, J. V. Pergolizzi, O. S. Cakmakkaya, and P. Kranke, "Transdermal scopolamine for the prevention of postoperative nausea and vomiting: A systematic review and meta-analysis," *Clinical Therapeutics*, vol. 32, pp. 1987-2002, 2010.
- [7] N. Rutter, "Applied physiology: the newborn skin," *Current Paediatrics*, vol. 13, pp. 226-230, 2003.
- [8] O. G. Jepps, Y. Dancik, Y. G. Anissimov, and M. S. Roberts, "Modeling the human skin barrier Towards a better understanding of dermal absorption," *Advanced Drug Delivery Reviews*, vol. 65, pp. 152-168, 2013.
- [9] A. M. Wokovich, S. Prodduturi, W. H. Doub, A. S. Hussain, and L. F. Buhse, "Transdermal drug delivery system (TDDS) adhesion as a critical safety, efficacy and quality attribute," *European Journal of Pharmaceutics and Biopharmaceutics*, vol. 64, pp. 1-8, 2006.

- [10] B. W. Barry, "Novel mechanisms and devices to enable successful transdermal drug delivery," *European Journal of Pharmaceutical Sciences*, vol. 14, pp. 101-114, 2001.
- [11] F. K. Akomeah, G. P. Martin, A. G. Muddle, and M. B. Brown, "Effect of abrasion induced by a rotating brush on the skin permeation of solutes with varying physicochemical properties," *European Journal of Pharmaceutics and Biopharmaceutics*, vol. 68, pp. 724-734, 2008.
- [12] X. M. Wu, H. Todo, and K. Sugibayashi, "Effects of pretreatment of needle puncture and sandpaper abrasion on the in vitro skin permeation of fluorescein isothiocyanate (FITC)-dextran," *International Journal of Pharmaceutics*, vol. 316, pp. 102-108, 2006.
- [13] W. R. Lee, S. C. Shen, K. H. Wang, C. H. Hu, and J. Y. Fang, "Lasers and microdermabrasion enhance and control topical delivery of vitamin C," *Journal of Investigative Dermatology*, vol. 121, pp. 1118-1125, 2003.
- [14] J. A. Mikszta, J. M. Brittingham, J. Alarcon, R. J. Pettis, and J. P. Dekker, "Topical delivery of vaccines," *United States Patent:* 6595947, 2003.
- [15] K. Sugibayashi, K. Hosoya, Y. Morimoto, and W. I. Higuchi, "Effect of the absorption enhancer, Azone, on the transport of 5-fluorouracil across hairless rat skin," *Journal of Pharmacy Pharmacology*, vol. 37, pp. 578-580, 1985.
- [16] A. C. Williams and B. W. Barry, "Penetration enhancers," *Advanced Drug Delivery Reviews*, vol. 64, Supplement, pp. 128-137, 2012.
- [17] S. del Rio-Sancho, C. E. S. Jiménez, M. A. C. Pascual, C. B. Fernández, A. F. Font, V. Merino, and A. L. Castellano, "Transdermal absorption of memantine effect of chemical enhancers, iontophoresis, and role of enhancer lipophilicity," *European Journal of Pharmaceutics and Biopharmaceutics*, vol. 82, pp. 164-170, 2012.
- [18] S. Henry, D. V. McAllister, M. G. Allen, and M. R. Prausnitz, "Microfabricated microneedles: a novel approach to transdermal drug delivery," *Journal of Pharmaceutical Sciences*, vol. 87, pp. 922-925, 1998.
- [19] P. Khanna, B. R. Flam, B. Osborn, J. A. Strom, and S. Bhansali, "Skin penetration and fracture strength testing of silicon dioxide microneedles," *Sensors and Actuators A: Physical*, vol. 170, pp. 180-186, 2011.
- [20] B. P. Chaudhri, F. Ceyssens, T. Guan, A. La Manna, H. P. Neves, C. Van Hoof,

- and R. Puers, "High strength, polymer microneedles for transdermal drug delivery," *Procedia Engineering*, vol. 25, pp. 1377-1380, 2011.
- [21] Y. Ito, H. Murano, N. Hamasaki, K. Fukushima, and K. Takada, "Incidence of low bioavailability of leuprolide acetate after percutaneous administration to rats by dissolving microneedles," *International Journal of Pharmaceutics*, vol. 407, pp. 126-131, 2011.
- [22] M. Pearton, S. M. Kang, J. M. Song, Y. C. Kim, F. S. Quan, A. Anstey, M. Ivory, M. R. Prausnitz, R. W. Compans, and J. C. Birchall, "Influenza virus-like particles coated onto microneedles can elicit stimulatory effects on Langerhans cells in human skin," *Vaccine*, vol. 28, pp. 6104-6113, 2010.
- [23] F. Chabri, K. Bouris, T. Jones, D. Barrow, A. Hann, C. Allender, K. Brain, and J. Birchall, "Microfabricated silicon microneedles for nonviral cutaneous gene delivery," *British Journal of Dermatology*, vol. 150, pp. 869-877, 2004.
- [24] D. V. McAllister, P. M. Wang, S. P. Davis, J. H. Park, P. J. Canatella, M. G. Allen, and M. R. Prausnitz, "Microfabricated needles for transdermal delivery of macromolecules and nanoparticles: Fabrication methods and transport studies," *Proceedings of the National Academy of Sciences of the United States of America*, vol. 100, pp. 13755-13760, 2003.
- [25] J. Gupta, H. S. Gill, S. N. Andrews, and M. R. Prausnitz, "Kinetics of skin resealing after insertion of microneedles in human subjects," *Journal of Controlled Release*, vol. 154, pp. 148-155, 2011.
- [26] Y. C. Kim, J. H. Park, and M. R. Prausnitz, "Microneedles for drug and vaccine delivery," *Advanced Drug Delivery Reviews*, vol. 64, pp. 1547-1568, 2012.
- [27] Y. Xie, B. Xu, and Y. Gao, "Controlled transdermal delivery of model drug compounds by MEMS microneedle array," *Nanomedicine: Nanotechnology, Biology and Medicine*, vol. 1, pp. 184-190, 2005.
- [28] S. P. Davis, W. Martanto, M. G. Allen, and M. R. Prausnitz, "Hollow metal microneedles for insulin delivery to diabetic rats," *IEEE Transactions on Biomedical Engineering*, vol. 52, pp. 909-915, 2005.
- [29] W. Martanto, J. S. Moore, O. Kashlan, R. Kamath, P. M. Wang, J. M. O'Neal, and M. R. Prausnitz, "Microinfusion using hollow microneedles," *Pharmaceutical Research*, vol. 23, pp. 104-113, 2006.
- [30] P. M. Wang, M. Cornwell, J. Hill, and M. R. Prausnitz, "Precise microinjection

- into skin using hollow microneedles," *Journal of Investigative Dermatology*, vol. 126, pp. 1080-1087, 2006.
- [31] Q. Cui, C. Liu, and X. F. Zha, "Study on a piezoelectric micropump for the controlled drug delivery system," *Microfluidics and Nanofluidics*, vol. 3, pp. 377-390, 2007.
- [32] M. L. Reed and W. K. Lye, "Microsystems for drug and gene delivery," *Proceedings of the IEEE*, vol. 92, pp. 56-75, 2004.
- [33] K. van der Maaden, W. Jiskoot, and J. Bouwstra, "Microneedle technologies for (trans)dermal drug and vaccine delivery," *Journal of Controlled Release*, vol. 161, pp. 645-655, 2012.
- [34] J. W. Lee, J. H. Park, and M. R. Prausnitz, "Dissolving microneedles for transdermal drug delivery," *Biomaterials*, vol. 29, pp. 2113-2124, 2008.
- [35] A. Alexander, S. Dwivedi, Ajazuddin, T. K. Giri, S. Saraf, S. Saraf, and D. K. Tripathi, "Approaches for breaking the barriers of drug permeation through transdermal drug delivery," *Journal of Controlled Release*, vol. 164, pp. 26-40, 2012.
- [36] A. P. R. Kumar, "Modified transdermal technologies: breaking the barriers of drug permeation via the skin," *Tropical Journal of Pharmaceutical Research*, vol. 6, pp. 633-644, 2007.
- [37] V. Sachdeva, H. D. Kim, P. M. Friden, and A. K. Banga, "Iontophoresis mediated in vivo intradermal delivery of terbinafine hydrochloride," *International Journal of Pharmaceutics*, vol. 393, pp. 113-119, 2010.
- [38] M. A. C. Pascual, C. B. Fernández, C. E. S. Jiménez, S. Del R. Sancho, A. F. Font, V. Merino, and A. L. Castellano, "Effect of iontophoresis on in vitro transdermal absorption of almotriptan," *International Journal of Pharmaceutics*, vol. 416, pp. 189-194, 2011.
- [39] A. Djabri, R. H. Guy, and M. B. D. Charro, "Transdermal iontophoresis of ranitidine: An opportunity in paediatric drug therapy," *International Journal of Pharmaceutics*, vol. 435, pp. 27-32, 2012.
- [40] H. Chen, H. Zhu, J. Zheng, D. Mou, J. Wan, J. Zhang, T. Shi, Y. Zhao, H. Xu, and X. Yang, "Iontophoresis-driven penetration of nanovesicles through microneedle-induced skin microchannels for enhancing transdermal delivery of insulin," *Journal of Controlled Release*, vol. 139, pp. 63-72, 2009.

- [41] G. Qin, Y. Gao, Y. Wu, S. Zhang, Y. Qiu, F. Li, and B. Xu, "Simultaneous basal-bolus delivery of fast-acting insulin and its significance in diabetes management," *Nanomedicine: Nanotechnology, Biology and Medicine*, vol. 8, pp. 221-227, 2012.
- [42] G. L. Li, T. J. Van Steeg, H. Putter, J. Van Der Spek, S. Pavel, M. Danhof, and J. A. Bouwstra, "Cutaneous side-effects of transdermal iontophoresis with and without surfactant pretreatment: a single-blinded, randomized controlled trial," *British Journal of Dermatology*, vol. 153, pp. 404-412, 2005.
- [43] K. A. Stockwell, D. J. Virley, M. Perren, M. M. Iravani, M. J. Jackson, S. Rose, and P. Jenner, "Continuous delivery of ropinirole reverses motor deficits without dyskinesia induction in MPTP-treated common marmosets," *Experimental Neurology*, vol. 211, pp. 172-179, 2008.
- [44] P. A. Sloan, D. E. Moulin, and H. Hays, "A clinical evaluation of transdermal therapeutic system fentanyl for the treatment of cancer pain," *Journal of Pain and Symptom Management*, vol. 16, pp. 102-111, 1998.
- [45] L. G. Hemkens, U. Grouven, R. Bender, C. Günster, S. Gutschmidt, G. W. Selke, and P. T. Sawicki, "Risk of malignancies in patients with diabetes treated with human insulin or insulin analogues: a cohort study," *Diabetologia*, vol. 52, pp. 1732-1744, 2009.
- [46] R. Ruiter, L. E. Visser, M. P. P. van Herk-Sukel, J. W. W. Coebergh, H. R. Haak, P. H. Geelhoed-Duijvestijn, S. Straus, R. M. C. Herings, and B. H. C. Stricker, "Risk of cancer in patients on insulin glargine and other insulin analogues in comparison with those on human insulin: results from a large population-based follow-up study," *Diabetologia*, vol. 55, pp. 51-62, 2012.
- [47] S. C. L. Gough, "A review of human and analogue insulin trials," *Diabetes Research and Clinical Practice*, vol. 77, pp. 1-15, 2007.
- [48] F. Kennedy, "Recent developments in insulin delivery techniques," *Drugs*, vol. 42, pp. 213-227, 1991.
- [49] A. Rolla, "Pharmacokinetic and pharmacodynamic advantages of insulin analogues and premixed insulin analogues over human insulins: impact on efficacy and safety," *The American Journal of Medicine*, vol. 121, pp. S9-S19, 2008.
- [50] C. C. Lin, C. I. Li, S. Y. Yang, C. S. Liu, C. C. Chen, M. M. T. Fuh, W. Chen,

- and T. C. Li, "Variation of fasting plasma glucose: a predictor of mortality in patients with type 2 diabetes," *The American Journal of Medicine*, vol. 125, pp. 416.e9-416.e18, 2012.
- [51] G. Zoppini, G. Verlato, G. Targher, S. Casati, E. Gusson, V. Biasi, F. Perrone, E. Bonora, and M. Muggeo, "Is fasting glucose variability a risk factor for retinopathy in people with type 2 diabetes?," *Nutrition, Metabolism and Cardiovascular Diseases*, vol. 19, pp. 334-339, 2009.
- [52] S. C. Walpole, D. P. Merino, P. Edwards, J. Cleland, G. Stevens, and I. Roberts, "The weight of nations: an estimation of adult human biomass," *BMC Public Health*, vol. 12, pp. 439, 2012.
- [53] San Francisco Diabetes Teaching Center at the University of California,
  "Calculating insulin dose,"

  http://dtc.ucsf.edu/types-of-diabetes/type2/treatment-of-type-2-diabetes/medicati
  ons-and-therapies/type-2-insulin-rx/calculating-insulin-dose/#formulas.
- [54] M. E. Holmstrup, C. M. Owens, T. J. Fairchild, and J. A. Kanaley, "Effect of meal frequency on glucose and insulin excursions over the course of a day," *e-SPEN*, the European e-Journal of Clinical Nutrition and Metabolism, vol. 5, pp. 277-280, 2010.
- [55] C. L. Triplitt, "New technologies and therapies in the management of diabetes," *American Journal of Management Care*, vol. 13 Supplement 2, pp. 47-54, 2007.
- [56] R. K. Sivamani, B. Stoeber, G. C. Wu, H. Zhai, D. Liepmann, and H. Maibach, "Clinical microneedle injection of methyl nicotinate: stratum corneum penetration," *Skin Research and Technology*, vol. 11, pp. 152-156, 2005.
- [57] D. V. McAllister, P. M. Wang, S. P. Davis, J. H. Park, P. J. Canatella, M. G. Allen, and M. R. Prausnitz, "Microfabricated needles for transdermal delivery of macromolecules and nanoparticles: Fabrication methods and transport studies," *Proceedings of the National Academy of Sciences*, vol. 100, pp. 13755-13760, 2003.
- [58] N. Roxhed, B. Samel, L. Nordquist, P. Griss, and G. Stemme, "Painless drug delivery through microneedle-based transdermal patches featuring active infusion," *IEEE Transactions on Biomedical Engineering*, vol. 55, pp. 1063-1071, 2008.
- [59] A. Richter, C. Klenke, and K. F. Arndt, "Adjustable low dynamic pumps based

- on hydrogels," Macromolecular Symposia, vol. 210, pp. 377-384, 2004.
- [60] O. Wichterle and D. L m, "Hydrophilic gels for biological use," *Nature*, vol. 185, pp. 117-118, 1960.
- [61] K. Dušek and D. Patterson, "Transition in swollen polymer networks induced by intramolecular condensation," *Journal of Polymer Science Part A-2: Polymer Physics*, vol. 6, pp. 1209-1216, 1968.
- [62] K. Deligkaris, T. S. Tadele, W. Olthuis, and A. van den Berg, "Hydrogel-based devices for biomedical applications," *Sensors and Actuators B: Chemical*, vol. 147, pp. 765-774, 2010.
- [63] F. Brandl, F. Kastner, R. M. Gschwind, T. Blunk, J. Teßmar, and A. Göpferich, "Hydrogel-based drug delivery systems: Comparison of drug diffusivity and release kinetics," *Journal of Controlled Release*, vol. 142, pp. 221-228, 2010.
- [64] A. Naegel, M. Heisig, and G. Wittum, "Detailed modeling of skin penetration an overview," *Advanced Drug Delivery Reviews*, vol. 65, pp. 191-207, 2013.
- [65] H. Tu, Y. Qu, X. Hu, Y. Yin, H. Zheng, P. Xu, and F. Xiong, "Study of the sigmoidal swelling kinetics of carboxymethylchitosan-g-poly(acrylic acid) hydrogels intended for colon-specific drug delivery," *Carbohydrate Polymers*, vol. 82, pp. 440-445, 2010.
- [66] P. L. Ritger and N. A. Peppas, "A simple equation for description of solute release I. Fickian and non-fickian release from non-swellable devices in the form of slabs, spheres, cylinders or discs," *Journal of Controlled Release*, vol. 5, pp. 23-36, 1987.
- [67] J. T. Zhang, T. F. Keller, R. Bhat, B. Garipcan, and K. D. Jandt, "A novel two-level microstructured poly(N-isopropylacrylamide) hydrogel for controlled release," *Acta Biomaterialia*, vol. 6, pp. 3890-3898, 2010.
- [68] J. Gu, F. Xia, Y. Wu, X. Qu, Z. Yang, and L. Jiang, "Programmable delivery of hydrophilic drug using dually responsive hydrogel cages," *Journal of Controlled Release*, vol. 117, pp. 396-402, 2007.
- [69] A. Kumar, S. S. Lahiri, and H. Singh, "Development of PEGDMA: MAA based hydrogel microparticles for oral insulin delivery," *International Journal of Pharmaceutics*, vol. 323, pp. 117-124, 2006.
- [70] J. Wang, Z. Chen, M. Mauk, K. S. Hong, M. Li, S. Yang, and H. Bau, "Self-actuated, thermo-responsive hydrogel valves for lab on a chip," *Biomedical*

- Microdevices, vol. 7, pp. 313-322, 2005.
- [71] D. T. Eddington and D. J. Beebe, "A valved responsive hydrogel microdispensing device with integrated pressure source," *Journal of Microelectromechanical Systems*, vol. 13, pp. 586-593, 2004.
- [72] Y. A. Ismail, J. G. Mart nez, A. S. Al Harrasi, S. J. Kim, and T. F. Otero, "Sensing characteristics of a conducting polymer/hydrogel hybrid microfiber artificial muscle," *Sensors and Actuators B: Chemical*, vol. 160, pp. 1180-1190, 2011.
- [73] K. L. Yung, X. Yan, K. Chunlei, H. Liu, K. F. Tam, S. M. Ko, F. Y. Kwan, and M. H. L. Thomas, "Sharp tipped plastic hollow microneedle array by microinjection moulding," *Journal of Micromechanics and Microengineering*, vol. 22, p. 015016, 2012.
- [74] T. Caykara, M. Bulut, N. Dilsiz, and Y. Akyűz, "Marcoporous poly(acrylamide) hydrogels: swelling and shrinking behaviors," *Journal of Macromolecular Science, Part A: Pure and Applied Chemistry*, vol. 43, pp. 889-897, 2006.
- [75] K. Choonee, R. R. A. Syms, M. M. Ahmad, and H. Zou, "Post processing of microstructures by PDMS spray deposition," *Sensors and Actuators A: Physical*, vol. 155, pp. 253-262, 2009.
- [76] W. Y. Zhang, G. S. Ferguson, and S. T. Lucic, "Elastomer-supported cold welding for room temperature wafer-level bonding," *17th IEEE International Conference on Microelectromechanical Systems (MEMS)*, pp. 741-744, 2004.
- [77] A. M. Barbero and H. F. Frasch, "Pig and guinea pig skin as surrogates for human in vitro penetration studies: a quantitative review," *Toxicology in Vitro*, vol. 23, pp. 1-13, 2009.
- [78] A. El-Kattan, C. S. Asbill, and S. Haidar, "Transdermal testing: practical aspects and methods," *Pharmaceutical Science & Technology Today*, vol. 3, pp. 426-430, 2000.
- [79] M. Wei, L. Ong, M. T. Smith, F. B. Ross, K. Schmid, A. J. Hoey, D. Burstow, and L. Brown, "The streptozotocin-diabetic rat as a model of the chronic complications of human diabetes," *Heart, Lung and Circulation*, vol. 12, pp. 44-50, 2003.
- [80] Y. C. Ah, J. K. Choi, Y. K. Choi, H. M. Ki, and J. H. Bae, "A novel transdermal patch incorporating meloxicam: in vitro and in vivo characterization,"

- International Journal of Pharmaceutics, vol. 385, pp. 12-19, 2010.
- [81] G. Yan, K. S. Warner, J. Zhang, S. Sharma, and B. K. Gale, "Evaluation needle length and density of microneedle arrays in the pretreatment of skin for transdermal drug delivery," *International Journal of Pharmaceutics*, vol. 391, pp. 7-12, 2010.
- [82] E. Varghese and R. K. Khar, "Enhanced skin permeation of diclofenac by iontophoresis: in vitro and in vivo studies," *Journal of Controlled Release*, vol. 38, pp. 21-27, 1996.
- [83] J. Singh and M. E. Weber, "Kinetics of one-dimensional gel swelling and collapse for large volume change," *Chemical Engineering Science*, vol. 51, pp. 4499-4508, 1996.
- [84] F. Munarin, S. Bozzini, L. Visai, M. C. Tanzi, and P. Petrini, "Sterilization treatments on polysaccharides: Effects and side effects on pectin," *Food Hydrocolloids*, vol. 31, pp. 74-84, 2013.
- [85] E. Cottam, D. W. L. Hukins, K. Lee, C. Hewitt, and M. J. Jenkins, "Effect of sterilisation by gamma irradiation on the ability of polycaprolactone (PCL) to act as a scaffold material," *Medical Engineering & Physics*, vol. 31, pp. 221-226, 2009.
- [86] "Cost estimator for injection molding,"

  http://www.custompartnet.com/estimate/injection-molding/.
- [87] K. Kabiri, H. Omidian, S. A. Hashemi, and M. J. Z. Mehr, "Synthesis of fast-swelling superabsorbent hydrogels: effect of crosslinker type and concentration on porosity and absorption rate," *European Polymer Journal*, vol. 39, pp. 1341-1348, 2003.
- [88] P. D. Peeva, N. Million, and M. Ulbricht, "Factors affecting the sieving behavior of anti-fouling thin-layer cross-linked hydrogel polyethersulfone composite ultrafiltration membranes," *Journal of Membrane Science*, vol. 390-391, pp. 99-112, 2012.
- [89] H. N. Huang, T. L. Li, Y. L. Chan, C. L. Chen, and C. J. Wu, "Transdermal immunization with low-pressure-gene-gun mediated chitosan-based DNA vaccines against Japanese encephalitis virus," *Biomaterials*, vol. 30, pp. 6017-6025, 2009.
- [90] M. J. Garland, E. C. Salvador, K. Migalska, A. D. Woolfson, and R. F. Donnelly,

- "Dissolving polymeric microneedle arrays for electrically assisted transdermal drug delivery," *Journal of Controlled Release*, vol. 159, pp. 52-59, 2012.
- [91] Y. Mou, X. Jiang, Y. Du, and L. Xue, "Intelligent bioengineering in vitiligo treatment: transdermal protein transduction of melanocyte-lineage-specific genes," *Medical Hypotheses*, vol. 79, pp. 786-789, 2012.
- [92] J. M. Song, Y. C. Kim, P. G. Barlow, M. J. Hossain, K. M. Park, R. O. Donis, M. R. Prausnitz, R. W. Compans, and S. M. Kang, "Improved protection against avian influenza H5N1 virus by a single vaccination with virus-like particles in skin using microneedles," *Antiviral Research*, vol. 88, pp. 244-247, 2010.